GAS PERMEATION THROUGH NANOPOROUS POLYCARBONATE TRACK-ETCHED MEMBRANES: PULSED PLASMA POLYMERIZATION OF THIN COATINGS TO MODULATE GAS PERMEABILITY

by

CHRISTOPHER LEWIS CHAPMAN

Presented to the Faculty of the Graduate School of

The University of Texas at Arlington in Partial Fulfillment

of the Requirements

for the Degree of

MASTER OF SCIENCE IN BIOMEDICAL ENGINEERING

THE UNIVERSITY OF TEXAS AT ARLINGTON

AUGUST 2007

ACKNOWLEDGEMENTS

I would like to thank Dr. Chuong for giving me a chance to work on this exciting project. I'd also like to thank Dr. Eberhart and Dr. Timmons for their guidance and expertise. This was a project with multiple collaborators involved in many departments. I'd like to thank all the collaborators. Special gratitude goes to Dhiman Bhattacharyya for his plasma coating expertise. I'd like to thank Anna for her support. Finally, I thank my mother for all her love and encouragement.

This research was supported in part by ORtech, Bioengineering, Inc., AFOSR FA-9550-06-0413, Collaborative UTA/SPRING Research & Nanotechnology Transfer Program and MRCEDM grants.

July 23, 2007

ABSTRACT

GAS PERMEATION THROUGH NANOPOROUS POLYCARBONATE TRACK-ETCHED MEMBRANES: PULSED PLASMA POLYMERIZATION OF THIN COATINGS TO MODULATE GAS PERMEABILITY

Publication No. _____

Christopher Lewis Chapman, M.S.

The University of Texas at Arlington, 2007

Supervising Professor: Dr. Cheng-Jen Chuong

Polycarbonate track-etched membranes (PCTE) of 50nm and 100nm pore size, precoated with Poly Vinyl Pyrrolidone (PVP), were surface treated with either Vinyl Acetic acid (VAA) or Perfluorohexane (C_6F_{14}) using a low duty cycle pulsed plasma polymerization technique. The effects of this surface treatment on gas permeation properties of the PCTE were addressed. Plasma coating thickness was controllably varied and resulted in gradual reduction of O_2 and CO_2 permeability as thickness increased from 10nm to 100nm. Plasma coating material, permeant gas, membrane pore size, and crosslink density were also varied in order to gain insight into the permeation properties of the PCTE. The results show the wide range of permeability achievable via this method. O_2 was more permeable than CO_2 as expected. Varying the

crosslink density had a noticeable effect on the gas permeability as well as the surface wettability. Also, the results from advancing/receding contact angle measurements indicate a much more hydrophobic character when the surface was coated with C_6F_{14} compared to the uncoated and VAA coated samples.

Blood oxygenation is an intended future application of this process. It was shown that the modified PCTE membranes had sufficient O_2 and CO_2 transfer for this purpose. This study supports the idea of utilizing the plasma polymerization process to modulate the gas permeability characteristics of the PCTE membranes and also alter the membrane surface to improve performance.

TABLE OF CONTENTS

LIST OF ILLUSTRATIONS

LIST OF TABLES

LIST OF NOMENCLATURE AND ABBREVIATIONS

A……..membrane area (cm^2)

AFM……atomic force microscope

C_6F_{14}……....perfluorohexane

CO_2…….....carbon dioxide gas

[COOH]……...carboxylic acid concentration

FIB……...focused ion beam

HE……....high energy

J……...flowrate (mL/s)

k…….…….Boltzmann's constant ($1.38x10^{-23}$J/K)

Kn……...…….…Knudsen number

L…….…….membrane thickness (um)

LE……....……low energy

MEMS…….microelectromechanical systems

M…….molecular weight (g/mol)

N_A……Avogadro's number ($6.02x10^{23}$ molecules)

O_2……oxygen gas

P……..operating pressure (psi)

PCTE…….……..polycarbonate track-etched

PNIPAm…….……poly-N-isopropyl (acryl-amide)

PVP…….poly vinyl pyrrolidone

R…….universal gas constant (8.314J/K/mol)

SEM……scanning electron microscopy

T…….absolute temperature (K)

VAA…….…..vinyl acetic acid

XPS…….……x-ray photoelectron spectroscopy

γ…….…….surface tension (mJ/m^2)

γ_{SV}…….……..surface tension between solid and vapor

ΔP……...……pressure differential (cmHg)

θ……...……contact angle (degrees)

θ_E……..……..equilibrium contact angle (degrees)

λ…….……gas mean free path (nm)

λ_p……membrane pore diameter (nm)

σ_A……collision diameter of gas A (Angstrom)

CHAPTER 1

INTRODUCTION

1.1 Membrane Background

The first recorded experiment on the transport of gases and vapors through synthetic membranes by Thomas Graham in 1829 laid the foundation for experimental research in membrane transport. Around 1855, Fick first quantitatively described transport across boundary layers through his theory of molecular transport [1]. Around that time, in 1856, Darcy discovered that flow rate through porous media was proportional to the pressure gradient applied [2]. Benchold later found quantitative relationships between physical membrane parameters such as bubble point, pore size, and surface tension and membrane performance [1, 3]. These contributions have provided deep insight into the mechanisms of gas transport through membranes. By the 1960s, membrane science was well established and a multitude of data on performance of polymers was available; however, most membranes were problematic and not sufficient for widespread use. Improvement and refinement of synthetic polymers throughout the 1980s gave rise to improvements in the understanding of membrane transport and presented the opportunity for membranes to be used in large scale processes. Recently, the emergence of nanotechnology and improved membrane fabrication and processing techniques has given the membrane transport community a new direction of scientific study, however; a complete theoretical description and

extensive empirical data are yet required to improve understanding of membrane technology.

1.2 Membrane Characteristics

A membrane may be loosely defined as a selective barrier between two phases [4]. The barrier properties depend both on the nature of the membrane as well as the permeant fluid. Membranes can be classified in different ways: biological or synthetic, porous or dense, or thick or thin, etc. Important characteristics of membranes include membrane thickness, surface area available for mass transfer, porosity, pore size, as well as chemical makeup and fabrication process. A membrane may be dense or porous or a combination of the two. One way to classify porous membranes is by pore size. Microfiltration membranes encompass a 0.1um to 1um size range. The classification is further broken down according to Table 1.1 below.

Table 1.1: Classification of Microfiltration Membranes by Pore Size [1]

Classification	**Pore size, nm**
Macropores	>50
Mesopores	2-50
Micropores	<2

Membranes are most commonly used industrially for gas separation purposes where a feed gas is separated into two pure streams. The permeability of a material, the ability of a fluid to pass through a selective barrier, usually a membrane, can be

described by various mechanisms. Regardless of the particular mechanism, the transfer of material across a membrane is gradient-driven. In other words, membrane transfer will not take place without a gradient in pressure, concentration, temperature, or electrical potential [5]. For instance, when a higher pressure is exposed to one side of the membrane, the material will be driven from the higher pressure side to the lower pressure side due to the gradient. Since authors report results in different units, usually in terms of either molar or volume quantities, Table 1.2 lists conversion factors to change from one set of units to the other. In many applications including gas permeation, membrane distillation, gas separation, cell separation, and filtration, the permeability of the membrane is the most important characteristic.

Table 1.2: Conversion Factors for Permeability Units [6]

Quantity	**Multiply**	**By**	**To get**
Permeability	Barrers	3.348×10^{-19}	kmol/(m*s*Pa)
Permeability	Barrers	4.810×10^{-8}	ft^3(STP)/(ft*psi*day)
Permeance	Barrers/cm	3.348×10^{-17}	kmol/(m^2*s*Pa)
Permeance	Barrers/cm	1.466×10^{-6}	ft^3(STP)/(ft^2*psi*day)

The permeation of liquids through membranes can be described by the Hagen-Poiseuille (viscous flow) equation but permeation of gases will be emphasized in this report. The permeation of gases through membranes depends both on the membrane material and structure as well as the properties of the permeant gas (es). For porous

membranes, either Knudsen flow, viscous (Poiseuille) flow, or a combination of the two called transition flow describes the transfer of gases through the membrane [2, 3]. These transport mechanisms are illustrated in Figure 1.3. In nonporous membranes, a solution-diffusion model can used to describe the transport of gases but porous membrane transport is emphasized here. Information on other types of membrane transport may be found in [5, 7].

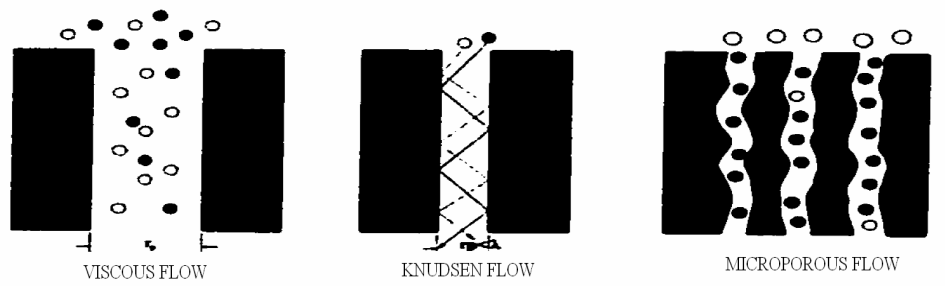

Figure 1.1: Illustration of gas transport models through porous media (adapted from [6])

When working with porous media it is desirable first to assess the relationship between pore size (λ_p) and mean free path (λ) of permeant gas. The Knudsen number, *Kn* is defined as the ratio λ / λ_p**.** The characteristic diameter in the mean free path is the collision diameter (σ_A) of the gas molecule. From the kinetic theory of gases, σ_A can be calculated as

$$\sigma_A^2 = \frac{5\left(\frac{MRT}{\pi}\right)^{1/2}}{16 N_A \mu} \qquad \text{(Eq. 1)}$$

where M is molecular weight, R is the universal gas constant, T is absolute temperature, N_A is Avogadro's number and μ is fluid viscosity. To calculate λ we use the following equation:

$$\lambda = \frac{kT}{\sqrt{2}\pi\sigma_A^2 P} \quad \text{(Eq.2)}$$

where k is Boltzmann's constant, T is absolute temperature, and P is pressure. The Knudsen number *Kn* once again is:

$$Kn = \frac{\lambda}{\lambda_p} \quad \text{(Eq.3)}$$

If *Kn* is <<1 then this means the mean free path is very small compared to the pore diameter and molecule-wall collisions are not likely to occur. However, if *Kn* is >>1 then the mean free path is along the order of magnitude of the pore diameter and Knudsen flow will occur where gas molecules become more likely to collide with pore walls than neighboring gas molecules. Also λ has a strong dependence on operating pressure. At extremely low pressure, λ becomes very large and Knudsen flow begins to dominate. Once the appropriate flow regime is determined, one may use either the Hagen–Poiseuille equation, the Knudsen equation, or a combination of the two to model the gas transport through the porous membrane. In some cases, a slip term must be incorporated to properly describe the flow.

1.3 Contact Angle of Surfaces

Another important characteristic of porous membranes for some applications is its surface wettability. For clarity, the following terms are defined.

i. Surface tension (γ) – the energy that must be supplied to increase the surface area by one unit-> typically in units of mJ/m^2. Alternatively, γ is a force (per length) along a line where the force is parallel to the surface but perpendicular to the line -> typically in units of mN/m. Note that the units mJ/m^2 and mN/m are identical.

ii. Surface energy- the interaction between the forces of cohesion and the forces of adhesion which determines whether or not wetting, the spreading of a liquid over a surface, occurs.

iii. Contact angle (θ) – the angle at which a liquid/vapor interface meets a solid surface.

iv. Wetting- the contact between a fluid and a surface, when the two are brought into contact.

The wettability of a porous membrane surface can be important in cases when a liquid is to be exposed to the membrane but not allowed to "seep" through the pores. In the case of porous membranes a hydrophilic, or water loving surface will allow water penetration through membrane pores. In contrast, a hydrophobic, or water-hating surface will resist penetration of water. Tailoring of membrane surface chemistry, namely the surface energy could change a hydrophobic material to hydrophilic and vice versa.

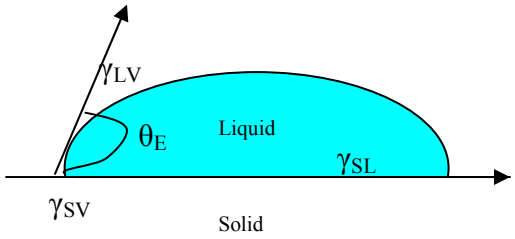

Figure 1.2: Illustration of the contact angle of a drop of liquid on a solid substrate

Figure 1.2 above illustrates the equilibrium contact angle, $\theta_{E,}$ measured on a liquid drop. This angle can be measured using a goniometer. Generally, there are two types of surfaces:

1. High energy (HE) surfaces- those for which the chemical binding energy is on the order of 1eV, on which nearly any liquid spreads. Theses surfaces are made of materials that are ionic, covalent, or metallic. The interface tension is given by

$$\gamma_{SV} \approx \frac{E_{binding}}{a^2} \approx 500 - 5000\, {mN}/{m}$$

2. Low energy (LE) surfaces- chemical binding energy on the order of kT (Boltzmann's constant multiplied by absolute temperature) and these are hardly wettable surfaces. These include materials such as molecular crystals and plastics. In this case,

$$\gamma_{SV} \approx \frac{kT}{a^2} \approx 10 - 50\, {mN}/{m}$$

The energy of the surface is directly related to the hydrophilic/hydrophobic nature of the surface. Consider a droplet of water in contact with a hydrophilic porous surface. It

can be imagined that some liquid escapes from the liquid drop and penetrates into the "nooks and crannies" of the solid. Ultimately, the drop finds itself on a wet surface seen as patches of solid and liquid as depicted in Figure 1.3 below. At the opposite extreme, consider a water droplet contacting a hydrophobic porous surface.

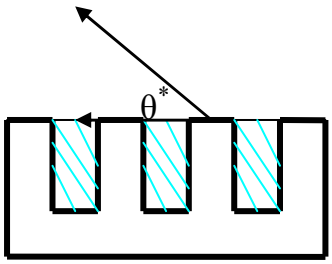

Figure 1.3: Hydrophilic porous surface on which the liquid may fill the pores and the drop will find itself on a mixed solid/ liquid surface

In this situation it is not necessarily expected for the liquid drop to fill or enter the membrane pores [8, 9]. Air can remain trapped in the pores under the drop. If so, the water drop rests on a composite surface of both solid and, air as shown in Figure 1.4 below.

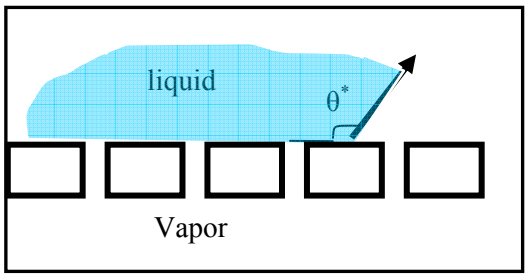

Figure 1.4: Hydrophobic porous surface on which the liquid does not necessarily fill the pores and the drop rests on a composite of solid and air

Simply by measuring the contact angle, one can gain valuable insight into the wetting properties of a surface. A static contact angle measurement may not be sufficient however in "telling the whole story" about the wettability of a surface. For

these situations, an advancing/receding contact angle technique may be implemented. In this technique a drop of water is first placed on the surface and the contact angle is measured just as in the static experiment. Next, the volume of the water droplet is incrementally increased and contact angle is recorded at each increment. Then to recede, the water volume is incrementally decreased. This results in information about the dynamic nature of the wettability of water on the surface.

1.4 Motivation for Research

An important application of membrane mass transfer is in blood oxygenator devices. Blood oxygenators have seen increased clinical use and research focus since the first prototype developed by Kolff in 1955 with polypropylene sheets [10]. They have been a leading topic of research in bioengineering for about 50 years now with little or no significant improvements in the last 20 years or so. Early oxygenator designs such as the film and rotating disc oxygenators found limited success. From the 1950s until the 1980s, the bubble oxygenator was the most widely used but still needed improvements. Beginning in the 1980s, the implementation of membrane oxygenators paved way for some improvements in oxygenator performance; however, they were still fraught with problems such as plasma leakage, hemolysis, and generally produced insufficient gas exchange [11]. Membranes are advantageous for this application since in order to reduce blood trauma, a physical barrier separating the blood phase from the gas phase is necessary. This is similar in some ways to the human lung which provides a massively large surface area, about $70m^2$, for transfer of oxygen into the blood and removal of CO_2; this transfer takes place across a blood gas barrier or membrane. In

cases of acute respiratory distress syndrome and other lung pathologies, the lung's inability to provide sufficient gas exchange may become fatal. To combat this, blood oxygenators replenish oxygenated blood to assist the lung in providing proper oxygenation to the body. Both dense and porous membranes have been investigated for oxygenator applications [10-12]. This barrier or membrane must allow the transfer of oxygen and carbon dioxide from one side of the membrane to the other but not allow any transfer of blood plasma from one side to the other.

New techniques such as MEMS fabrication and nanotechnology have brought new tools to the bioengineering realm. In particular, these tools have created the opportunity to develop devices more suitable to physiological dimensions to better mimic natural body processes. The original goal of this research project was of a collaborative effort to develop a novel nanoporous microchannel membrane blood oxygenator. Specifically, it was desired to characterize the gas transport across a microfabricated silicon/silicon nitride membrane as this would be the membrane fabricated for use in the blood oxygenator device. An important advantage of this design is that the silicon material is much stronger compared to other polymeric membranes. As a result, the high material strength and the fabrication techniques allow the creation of an incredibly thin blood channel, minimizing gas transfer resistance through the membranes and into the red blood cells. The silicon nitride membrane is made nanoporous by "drilling" holes using focused ion –beam (FIB) etching, yielding very straight and uniform pores. The membrane surface will be treated to tailor its hydrophobicity and improve biocompatibility. This treatment could alter the pore size

available for gas exchange and hence, alter its gas permeability. Given the inavailability of the silicon nitride membrane during the time period available for this thesis research and also to demonstrate feasibility, a surrogate membrane was chosen for gas transport studies. The surrogate of choice was polycarbonate track-etched membranes (PCTE).

Currently, PCTE membranes are used in various applications such as filtration, blood plasma separations, drug delivery, and flow control of reagents for assays [13, 14] but they have also been investigated for gas permeation/separation applications [15-20]. The PCTE membranes are fabricated by subjecting a thin film sheet of polycarbonate to energy neutron radiation applied perpendicular to the film. The particles damage the polymer and reduce polymer crosslinking, creating tracks. The film is then submerged into an acid or alkaline bath and the polymeric material is etched away along these tracks to form uniform cylindrical pores with a narrow pore size distribution. By varying fabrication operating conditions, a wide variety of pore sizes, from 20nm to 20um, are commercially available. PCTE membranes are unique in that they have rather uniform cylindrical pores of constant pore size as a result of this fabrication process. In other words, their pore morphology is very close to the ideal case of uniform straight cylindrical pores. This is the reason they were chosen as the surrogate material for preliminary study, their similarity in pore structure to the FIB etched silicon nitride which also closely represents an ideal case. In order to develop a suitable membrane for oxygenator applications, the optimum pore size and porosity of the gas-exchange membrane as well as the wettability of the membrane surface must be investigated. The surface tension of blood in the pores can not be so low that blood travels through the

pores from the blood side into the gas stream. This is called plasma "wet-out" and has been a problem for many oxygenators in the past. It is hoped that by both reducing pore sizes from the micron scale to the nanoscale as well as applying a hydrophobic coating to the pores, the wet-out phenomena will be further minimized or even prevented. With these objectives in mind, the gas permeation as well as the contact angle of the PCTE membranes have been studied.

1.5 Research Objectives

A simple experimental method and apparatus for determining gas permeability was implemented. Traditionally, these types of simple gas permeation methods on porous membranes were not very informative since detailed knowledge of the pore characteristics must be previously obtained in order to quantify the permeability accurately. PCTE membranes, as mentioned, have the benefit of a very uniform cylindrical pore structure and narrow pore size distribution of known value. As a result, traditional experimental techniques could be implemented since the pore structure represents a near ideal case of perfect cylindrical pores with a narrow range of pore sizes. The investigation of gas permeation characteristics through nanoporous track-etched polycarbonate membranes has led to some interesting findings.

Surface treatment of materials has become a popular tool for improving polymer performance by surface modification [21, 22]. In biomaterials, material surfaces are altered to improve compatibility with the body upon implantation. One common technique used to alter the surface properties is plasma polymerization. Plasma polymerization, by altering the surface of a substrate, can be used to improve

biocompatibility and increase gas separation performance [6, 23-26]. In the current study, PCTE membranes were coated to varying thickness via the low duty cycle pulsed plasma polymerization method. A plasma, or partially ionized gas produced by a high frequency electric field is used to bombard the substrate and alter its surface properties**.** The plasma coating was applied with the intent to coat the membrane pore walls thereby controllably decreasing the membrane pore size, ultimately resulting in a reduction in membrane permeability. Operating parameters such as monomer material, flow rate, pressure, and substrate location and temperature can be varied to adjust the plasma film chemistry [27]. The results from gas permeation experiments will indicate a gradual reduction of gas flux and hence, reduction of permeability through the PCTE membranes as plasma coating thickness increased. The pulsed plasma coatings were also used to alter the surface energy of the PCTE membranes to adjust hydrophobicity of membrane surface.

An extensive look into the effects of various parameters and operating conditions on permeability of PCTE membranes revealed an interesting hypothesis; suppose it was possible to apply a specific plasma coating so that a prescribed permeability could be achieved. It will be shown that the gas permeability can be regulated rather controllably to meet specified permeation needs by varying certain operating conditions in the plasma coating environment. The major parameters investigated were plasma coating thickness, plasma coating monomer (Vinyl Acetic Acid (VAA) or C_6F_{14}), type of permeant gas (CO_2 and O_2), uncoated membrane pore size (50nm and 100nm), and plasma polymerization crosslink density. These factors

were varied and compared in order to understand their effect on gas permeability and surface wettability of PCTE membranes as part of a grand effort to characterize the gas transfer characteristics of nanoporous membranes for application in blood oxygenation. The remaining sections of this report provide a general treatment of gas permeation properties through PCTE with out strict focus on a particular application, reinforcing the idea that this technology may be applicable to numerous fields.

CHAPTER 2

EXPERIMENTAL MATERIALS AND METHODS

2.1 Introduction

PCTE membranes (Sterlitech, Wisconsin) of 47mm diameter, with either 50nm or 100nm pore sizes, and thickness of 6um ±0.6 were utilized for this study. The PCTE membranes were subsequently coated either with C_6F_{14} or VAA (CH_2=$CHCH_2COOH$) via the pulsed plasma polymerization technique. A gas permeability apparatus was built to measure and compare the O_2 and CO_2 permeabilities of the PCTE membranes that were coated to varying degrees. The flowrate vs. pressure curves were obtained as raw data and after applying appropriate equations, the permeability was calculated. In addition to permeability studies, the PCTE membranes were also examined for their surface characteristics using the advancing/receding contact angle technique. Samples were also viewed under SEM to examine effects the of coatings on pore size and pore structure.

2.2 Coating of PCTE Membranes

PCTE membranes were purchased in 47mm diameter samples with nominal pore sizes of 50nm and 100nm. Samples were coated under varying conditions using the pulsed plasma polymerization technique. The gas flow rates as a function of applied pressure through coated and uncoated membranes were studied using a simple gas permeation apparatus described below. Also, the advancing/receding contact angle

measurements were taken to compare nanoporous surfaces with hydrophilic and hydrophobic coatings.

The PCTE membranes were coated via the low duty cycle pulsed plasma polymerization technique. A detailed description of the plasma reactor apparatus used has been described elsewhere [6, 22, 28]. Basically, three membranes at a time were placed in a cylindrical glass reactor and exposed to an ionized gas plasma that ultimately changed the surface of the substrate [25] . After sufficient reaction time (a few seconds to a few minutes) the resulting substrate should contain a uniform, conformal coating free of pinholes. Small square coupons of polished silicon were placed in the reactor environment along with the membranes to serve as controls for surface treatment. The coated silicon wafers were later used for profilometry measurement to determine film thickness and also used as controls for contact angle measurements. Operating conditions were varied in order to apply different coating thicknesses to the membrane surface. The plasma conditions have been well studied and in pulsed plasma polymerization the deposition time is usually linearly proportional to deposition thickness. The more time the sample spends in the reactor, the thicker the plasma coating becomes.

In addition to varying the conditions to adjust coating thickness, a separate study was conducted wherein the crosslink density was varied, also by manipulation of plasma reactor operating conditions. The crosslink density of the polymer film may be altered by adjusting power input as well as concentration of carboxylic acid [COOH] functional groups on the surface. Increasing polymer input increases crosslink density at

the risk of reducing surface functional groups. To optimize conditions to obtain reasonable crosslink density as well as sufficient functional groups, [COOH] content must be adjusted. This ultimately means that a lower [COOH] of functional groups available on the surface results in a higher crosslink density of polymer coating, an inverse relationship. For the present study three [COOH] of surface functional groups were compared; 8.9%, 5.6%, and 3.6% and are denoted for the remainder of the present paper as low, medium, and high crosslink density respectively. These [COOH] groups were verified by X-ray photoelectron spectroscopic characterization (XPS) [22, 28].

PCTE membranes containing 50nm or 100nm pore sizes were plasma coated with varying thicknesses from 10nm to 100nm with either Vinyl Acetic Acid (VAA) or Perfluorohexane (C_6F_{14}). Coated membranes were placed in vacuum for 2-3 days in order to remove any unreacted monomer content and subsequently set aside for gas permeation experiments.

2.3 Gas Permeability Experiments

2.3.1 Design of Gas Permeability Apparatus

The gas permeability apparatus, originally designed by Vance Ley [6], uses 1/4”and 1/8” steel Swagelok tubing as well as 1/8” flexible tubing that connects a gas cylinder source of either Oxygen gas or Carbon Dioxide gas (Airgas Southwest, Arlington, TX) to a digital pressure gauge (Cole Parmer, Illinois). From the gauge, the tubing feeds into a correlated flowmeter (Cole Parmer, Illinois) and immediately into the membrane chamber in which the membrane under study is securely sealed and mounted. A porous metal disc inside the membrane chamber is used to support the

PCTE membranes but does not have any noticeable impedance to gas flowrate. From the membrane chamber, the tubing connects to a glass bubble flowmeter (Bubble-O-Meter, Ohio). See Figure 2.1 for a schematic. Simply put, a pressure can be applied to the gas, gas will exit the regulator, flow into the membrane chamber with mounted membrane, through the membrane, and finally into the bubble flowmeter. A soap bubble is introduced into the gas stream to calculate the flowrate by timing the rise of the soap bubble through a known volume increment.

2.3.2 Membrane Permeability Measurements

Once membranes were placed and sealed into membrane holder, oxygen was passed through for about two minutes to remove any residual gases. Although the diameter of membranes is 47mm the effective diameter in the flow path once mounted was only 36mm. Next, the vent, used to purge the lines, was closed and a pressure of 0.25psi was applied to the membrane. The SI equivalent of psi is Pa where 101,325Pa = 14.7psi. The resulting flowrate was measured. Five flowrate measurements were taken at a given applied pressure. The pressure was then incrementally adjusted from 0.25psi up to around 3.5psi or when the bubble flowed too fast to obtain accurate measurements. The membrane was then either removed from the membrane holder or a different gas was tested. Either Oxygen (O_2) or Carbon Dioxide (CO_2) were used as permeant gases for these studies. Tested membranes were set aside for preparation of SEM examination or contact angle measurement.

Since different polymers were used to surface treat the nanoporous PCTE membranes, the question of surface wettablity differences needed to be addressed.

Advancing/receding contact angle measurements were used to point out the differences these surface coatings made on the water contact angle, a direct measure of the wettablility of a surface. PCTE membranes before surface treatment are denoted "uncoated" although the membranes actually have a rather hydrophilic poly-vinyl-pyrrollidione (PVP) wetting agent applied at the manufacturing plant.

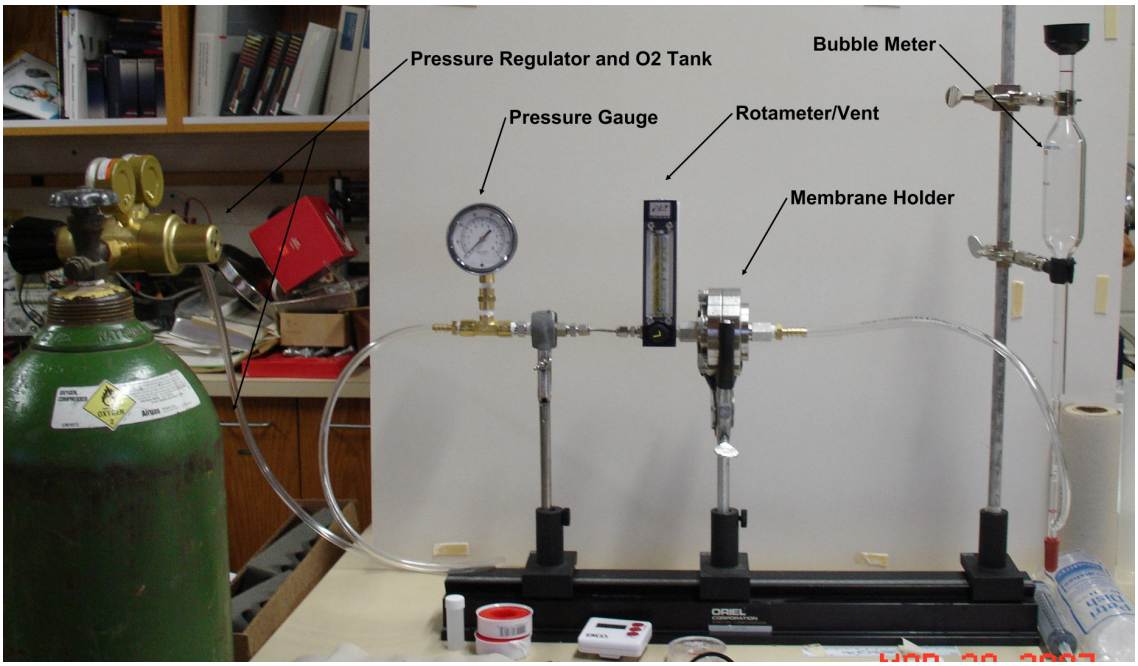

Figure 2.1: Photograph of the gas permeability apparatus

2.3.3 Treatment of Data

The flowrate of the gas exiting the membrane was experimentally measured, as described above, over a range of applied pressures up to around 3.5psi. After averaging the five flowrate measurements at each pressure, the resulting flow rate profile was plotted against pressure and a linear trendline was calculated to check for good correlation. In order to determine the gas permeability from the flowrate vs. pressure

curve, the slope of the linear trendline was calculated and the following equation was used:

$J = KA\frac{\Delta P}{L}$, where (Eq.4)

J= flowrate (mL/s)

A = membrane area exposed to gas stream (cm^2)

ΔP = pressure gradient (cmHg)

L = thickness of membrane (cm)

K= Permeability ($cm^3*cm*cm^{-2}*s^{-1}*cmHg^{-1}$)

Permeability is be expressed in Barrers where 1Barrer=$10^{-10}cm^3*cm*cm^{-2}*s^{-1}*cmHg^{-1}$. Since, in the preceding equation the volume flowrate through the membrane is proportional to the pressure difference applied across the membrane, then the permeability may be obtained from the slope of the flowrate vs. pressure line for a given membrane sample. For a plot of J vs. ΔP, the slope is equal to:

$Slope = \frac{KA}{L}$, so the permeability, K is:

$K = Slope * \frac{L}{A}$ (Eq. 5)

The permeability of the entire set of membranes was determined by the prescribed method and various parameters were compared.

2.4 Advancing/Receding Contact Angle Experiments

A Rame-Hart Goniometer (Rame-Hart Instrument Company, NJ) was used to measure the water contact angle on uncoated and pulsed plasma coated PCTE

membranes. Advancing/receding contact angle measurements were taken. The featured membrane was taped onto a clean glass slide so that the membrane lay extremely flat. For advancing/receding measurements, a 2uL water droplet was placed on the membrane surface. With the pipette tip submerged into the droplet, increments of 2uL were released into the droplet causing an increasingly larger water droplet. The contact angle was recorded at each volume increment. For the receding angle, the reverse process was performed: the micropipette was used to withdraw 2uL increments of water back from the droplet until the droplet was gone or the contact angle dropped below 20^0. The contact angle again was recorded at each volume increment. The resulting advancing/receding contact angle plots were used to compare hydrophobicity of membrane surfaces.

2.5 SEM Examination

SEM analysis was performed in order visualize the mircoscale structure of the nanoporous PCTE plasma coated membranes with various coating thickness. The membranes were first gold sputter-coated with a thickness around 70A using a MRC sputter coater system (Semicore, CA) to prevent charging. The membranes were then mounted onto sample studs and placed in the Zeiss Supra VP Scanning Electron Microscope (Zeiss, NY). Images were taken at 5 kV and 35kx and 50k magnification.

Table 2.1 below offers an overall summary of the aspects investigated and variables compared in the present study.

Table 2.1: Summary of Experiments Performed on PCTE Membranes and Aspects Investigated

PCTE membrane	Diameter: 47mm Effective Diameter 36mm Thickness 6um±0.6	**Gas Permeation**	**Contact Angle**	**SEM**
Coating Thickness	10-60nm for 50nm pore membranes 20-100nm for 100nm pore membranes	✓	✓	✓
Coating material	VAA, C_6F_{14}	✓	✓	VAA only
Permeant gas	O_2, CO_2	✓		
Pore diameter	50nm, 100nm	✓	✓	
Crosslink density	Low, medium, high	✓	✓	

CHAPTER 3

RESULTS

3.1 Gas Permeability Measurements

The purchased PCTE membranes were pulsed plasma coated to varying thicknesses as previously described. The flowrate vs. pressure curves for all samples were linear regressed and the slope was recorded. The gas permeability was determined using the appropriate equations (refer to section 2.3.3). To support the idea that gas permeability through PCTE membranes can be modulated by applying specific plasma coatings; the effects of plasma coating thickness, coating material, permeant gas, membrane pore size, and polymer cross-link density on membrane permeability are illustrated below. In addition, the resulting plots from contact angle measurements comparing different plasma coating materials will be presented. To assess the repeatability of measurements Figure 3.1 shows the flowrate vs. pressure line for n=6 untreated 50nm pore-sized samples with close agreement (r^2=0.9949). This variation is due to small measurement errors as well as variations in the PCTE samples themselves.

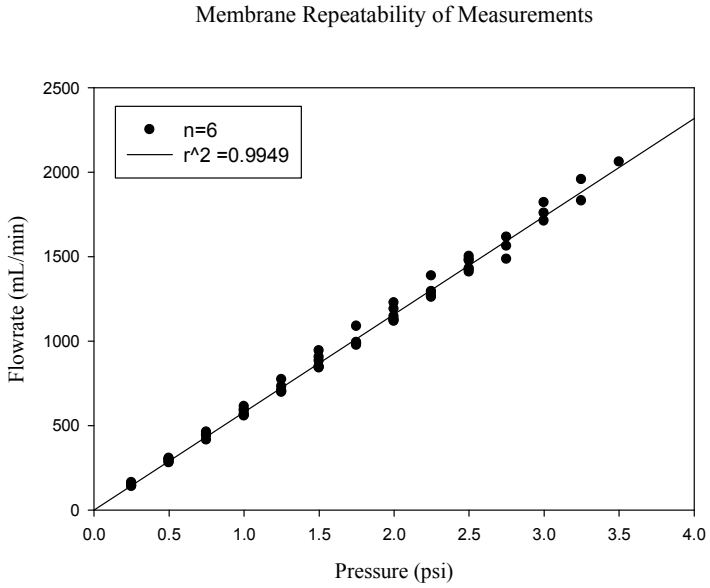

Figure 3.1: Flowrate vs. pressure curve for uncoated 50nm pore sized PCTE membranes

3.1.1 Effect of Coating Thickness

Plasma coatings 10nm to 60nm thick were applied to the 50nm pore-sized PCTE membranes and Figure 3.2 shows the resulting volume flowrate vs. pressure curves for VAA coated samples (n=3) at each coating thickness. A linear regression was calculated for each coating thickness and good correlation was observed. From the slope of the trendline, the gas permeability was calculated as described. In Figure 3.3 the permeability is plotted for a range of pressures for various VAA coatings. Figure 3.4 describes how the VAA coating thickness induces a gradual reduction in gas permeability through the PCTE membranes. A second-order polynomial with r^2=0.9729 was fit to the data to quantify how increasing coating thickness possibly correlates with permeability reduction. In contrast to the 50nm membranes displaying this polynomial

trend, the permeability vs. coating thickness for the 100nm membranes seemed to follow a more linear trend shown in Figure 3.5.

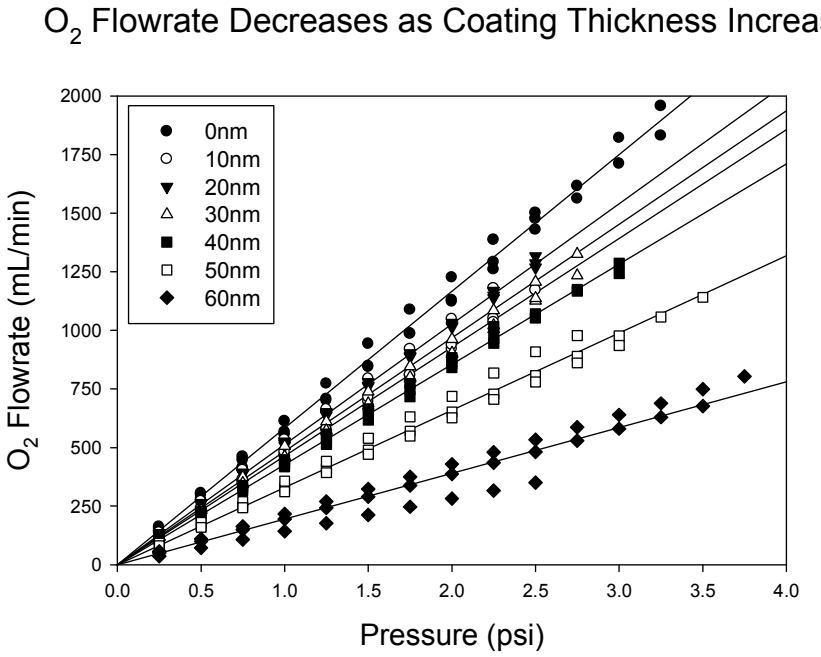

Figure 3.2: Linear regression of flowrate vs. pressure plots for 0-60nm VAA coatings (n=3) on 50nm pore sized PCTE membranes

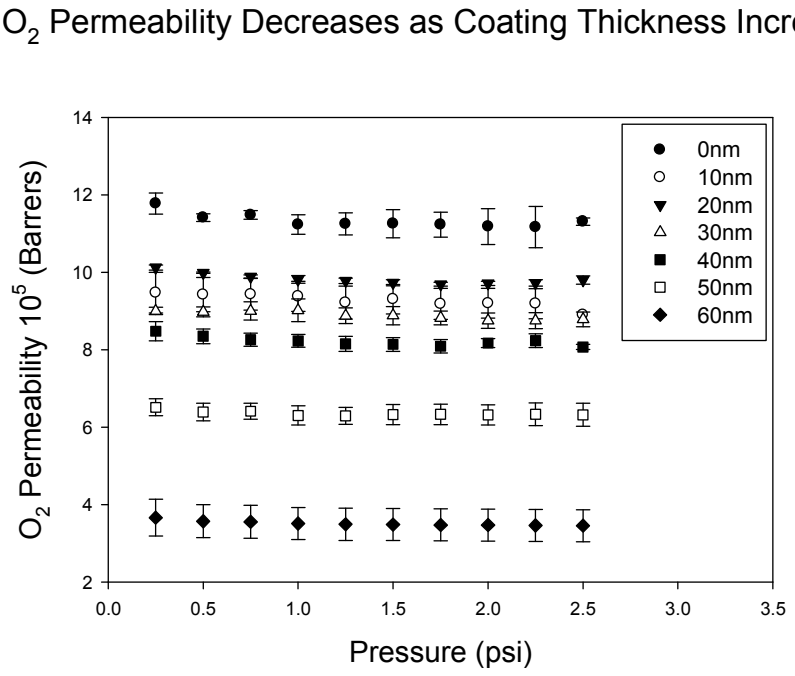

Figure 3.3: Permeability vs. pressure for 0-60nm VAA coatings (n=3) on 50nm pore sized PCTE membranes

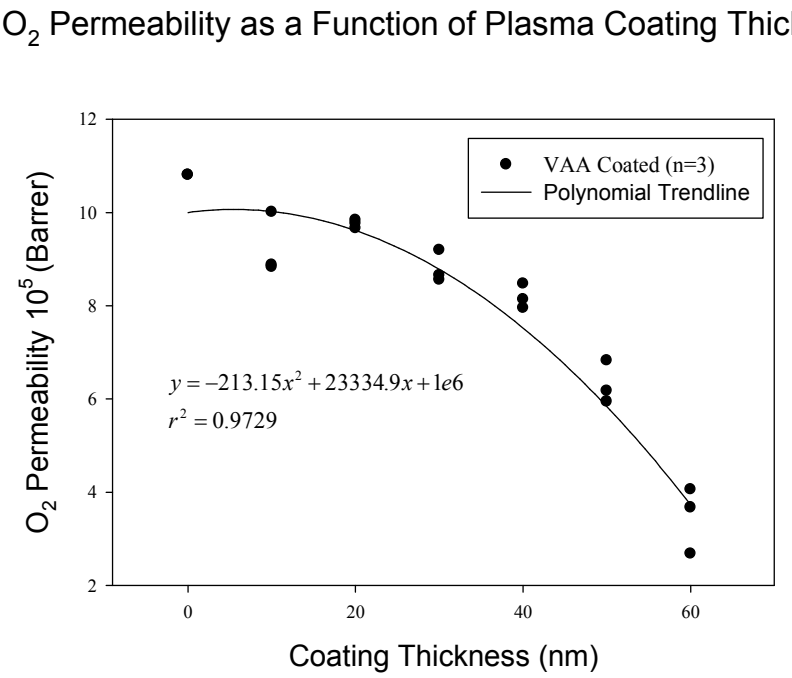

Figure 3.4: Plot of O_2 permeability through 50nm pore sized PCTE membranes with 0-60nm VAA coating thicknesses with polynomial curve fit

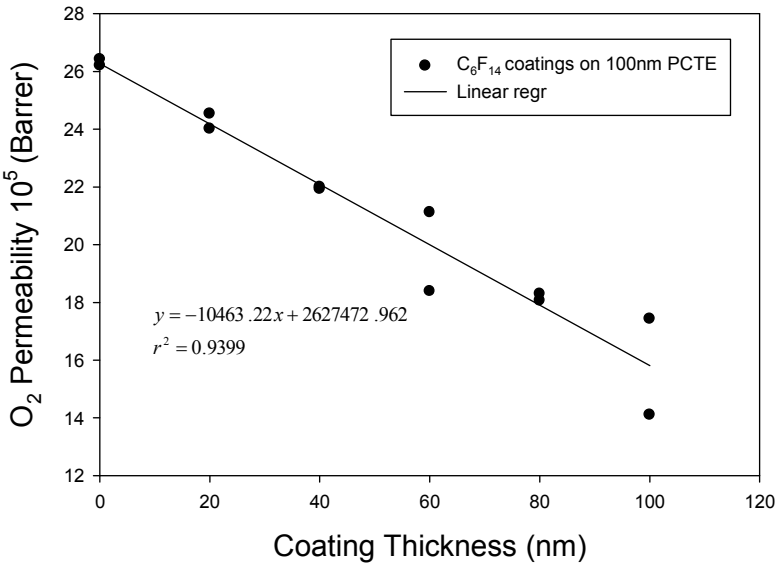

Figure 3.5: Plot of O_2 permeability through 100nm pore sized PCTE membranes with 0-100nm C_6F_{14} coating thicknesses with linear curve fit

3.1.2 Coating Material

Vinyl Acetic Acid (VAA) and perfluorohexane (C_6F_{14}) were employed as monomers for the plasma polymerization reactions. Polymeric C_6F_{14} and VAA coatings were deposited onto the PCTE membranes and subsequent gas permeability experiments were performed. In Figure 3.6, three membrane samples of each coating thickness, with either VAA or C_6F_{14} plasma coatings are presented as mean ± standard error. The differences these coating materials make on the membranes will become apparent in the contact angle analysis.

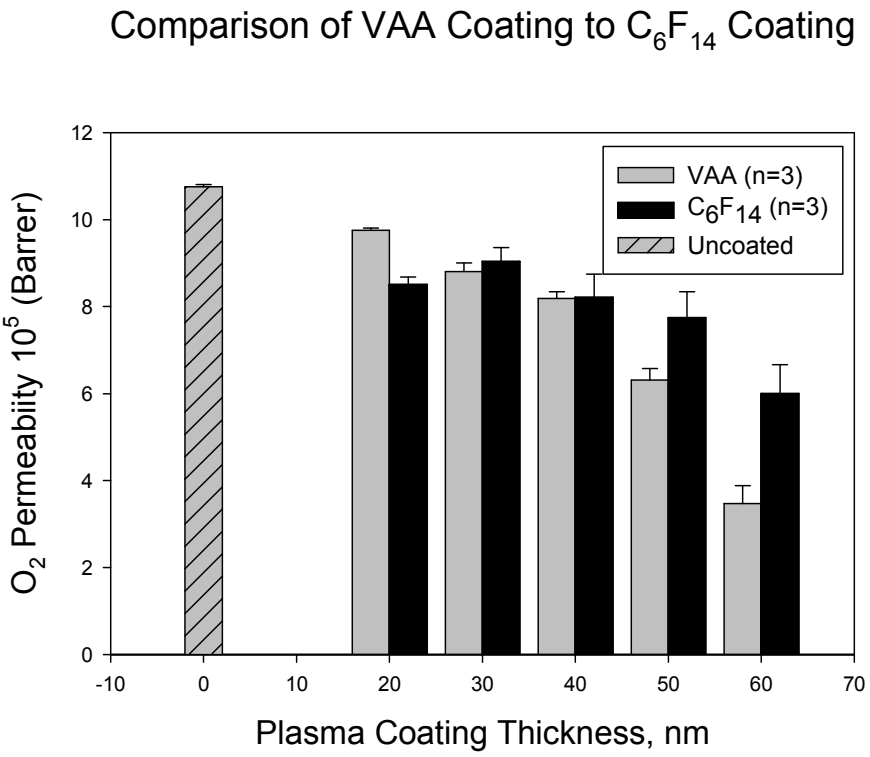

Figure 3.6: Vertical bar graph depicting O_2 permeability through 50nm pore sized PCTE membranes with 0-60nm VAA (n=3) and C_6F_{14} (n=3) coating thicknesses

3.1.3 Permeant Gas

Oxygen (O_2) and Carbon Dioxide (CO_2) gas were chosen as permeant gases for the membrane permeability experiments. To develop a comparison of these two permeant gases it is helpful to look at the Knudsen number, a ratio of mean free path of the gas to pore diameter. This will help to determine what flow regimes can be used to describe the gas transport through the membrane. If Knudsen flow dominates, then gas molecules find themselves colliding with the pore walls more often than with each other. The opposite is the case in viscous flow. If the Knudsen number lies in the range of unity then a transition regime with contributions from both the Knudsen flow and viscous flow will occur. The characteristic diameter in the mean free path is the collision diameter (σ_A) and it will be calculated first. *Kn* is simply the ratio λ / λ_p and it's value will follow. From the kinetic theory of gases, σ_A for O_2 molecules at room temperature is found by

$$\sigma_A^2 = \frac{5\left(\frac{MRT}{\pi}\right)^{1/2}}{16 N_A \mu} = \frac{5\left(\frac{\left(32\frac{g}{mol}\right)\left(8.314\frac{J}{K*mol}\right)(298K)}{\pi}\right)^{1/2}}{16\left(6.0223x10^{23}\frac{molec}{mol}\right)\left(0.0002\frac{dynes*s}{cm^2}\right)} = 1.30x10^{-19}\,m^2$$

$$\sigma_A = 3.61x10^{-10}\,m \;\; or \;\; 3.61A \qquad \text{(Eq.6)}$$

where M is molecular weight, R is the universal gas constant, T is temperature, N_A is Avogadro's number and μ is fluid viscosity. The mean free path λ was calculated from:

$$\lambda = \frac{kT}{\sqrt{2}\pi\sigma_A^2 P} = \frac{1.38x10^{-23}\,\frac{J}{K}}{\sqrt{2}\pi(3.61A)^2(1.51psi)} = 13.609nm \qquad \text{(Eq.7)}$$

where k is Boltzmann's constant, T is absolute temperature, and P is pressure. *Kn* for 100nm pores will be:

$$Kn = \frac{\lambda}{\lambda_p} = \frac{13.609nm}{100nm} = 0.13609 \qquad \text{(Eq.8)}$$

Kn for O_2 at a typical operating pressure of around 1.5psi is 0.136. Since the molecular weight of CO_2 is 44g/mol compared to 32g/mol for O_2, *Kn*=0.116 for CO_2 at the same conditions. The higher membrane permeability of O_2 over CO_2 is described in Figure 3.7 for 20nm to 60nm C_6F_{14} coatings on the PCTE. In Figure 3.8 the linear relationship between O_2 and CO_2 permeability through 50nm pore sized C_6F_{14} coated membranes is described with a linear trendline (r^2=0.989). The slope of the trendline was calculated to be 1.1671, the significance of which will be discussed in the next chapter. There is no respective plot for VAA-coated membranes since both gases were not tested on all VAA-coated samples.

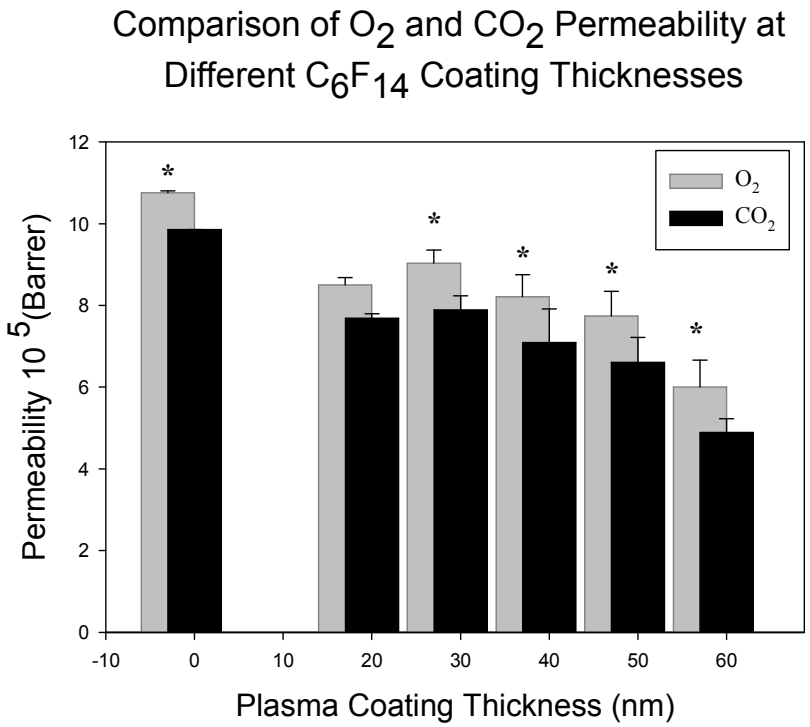

Figure 3.7: Comparison of O_2 and CO_2 permeability through 50nm pore sized PCTE membranes with 0-60nm VAA coating thicknesses with standard error

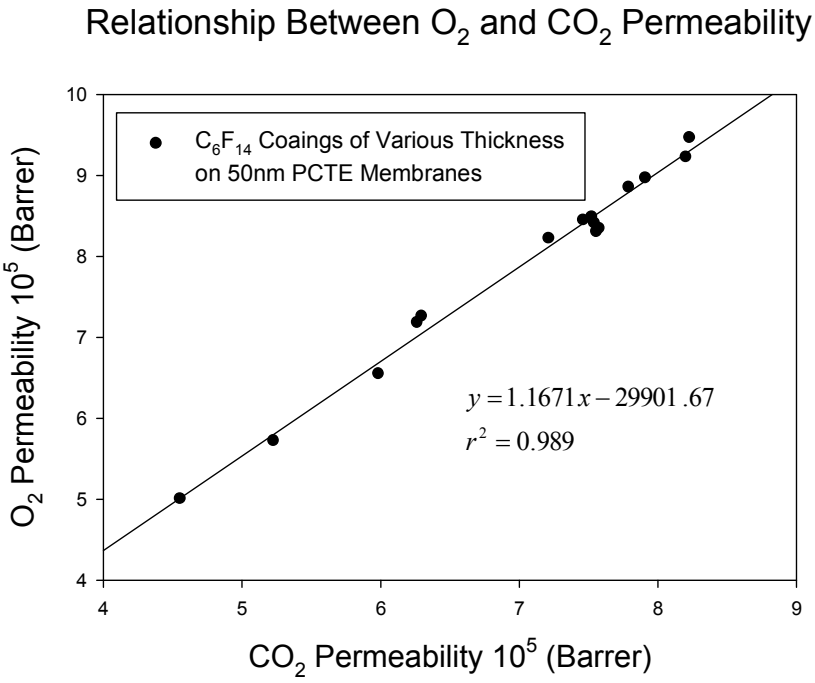

Figure 3.8: Linear curve fit of O_2 and CO_2 permeability through 50nm pore sized PCTE membranes with 0-60nm C_6F_{14} coating thicknesses

3.1.4 Membrane Pore Size

PCTE membranes with 50nm and 100nm pores were compared for their relative gas permeabilities. In Figure 3.9 the flowrate vs. pressure curves for 50nm and 100nm membranes are plotted. This plot comprises data points from all C_6F_{14} coating thicknesses. The flowrates obtained ranged from around 200-2000 mL/min to around 70-1200mL/min for 100nm and 50nm pore-sized membranes, respectively. Figure 3.10 shows the permeability values obtained for each coating thickness and how they vastly differ when comparing PCTE membranes with 50nm pores to those with 100nm pores. The PCTE membranes with 50nm pores were coated with thicknesses at 10nm increments from 20-60nm whereas the membranes with 100nm pores were coated at 20nm increments from 20-100nm coating thicknesses. Permeability values from $5x10^5$ to $2.5x10^6$ Barrers were calculated.

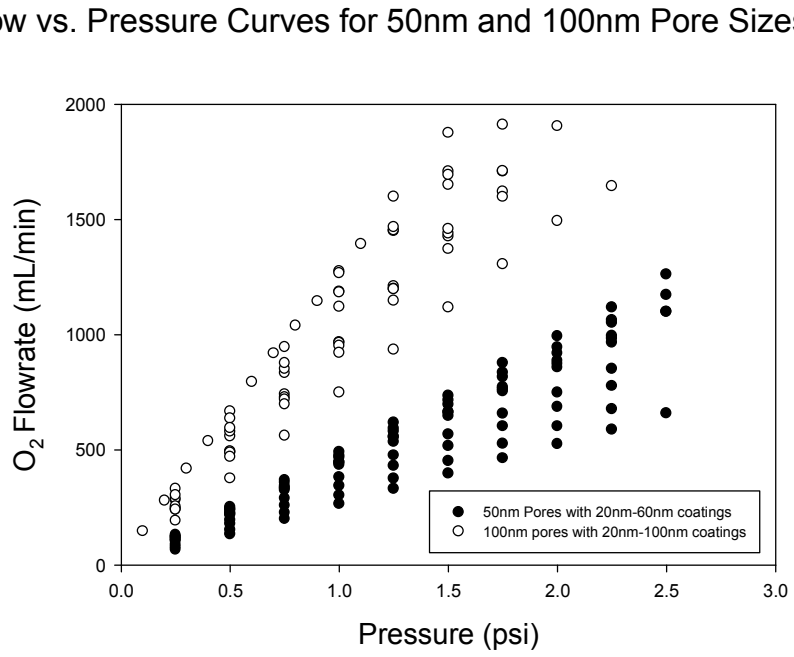

Figure 3.9: Flowrate vs. pressure curves for PCTE membranes with 50nm and 100nm pores coated with 20-100nm C_6F_{14} coating thicknesses

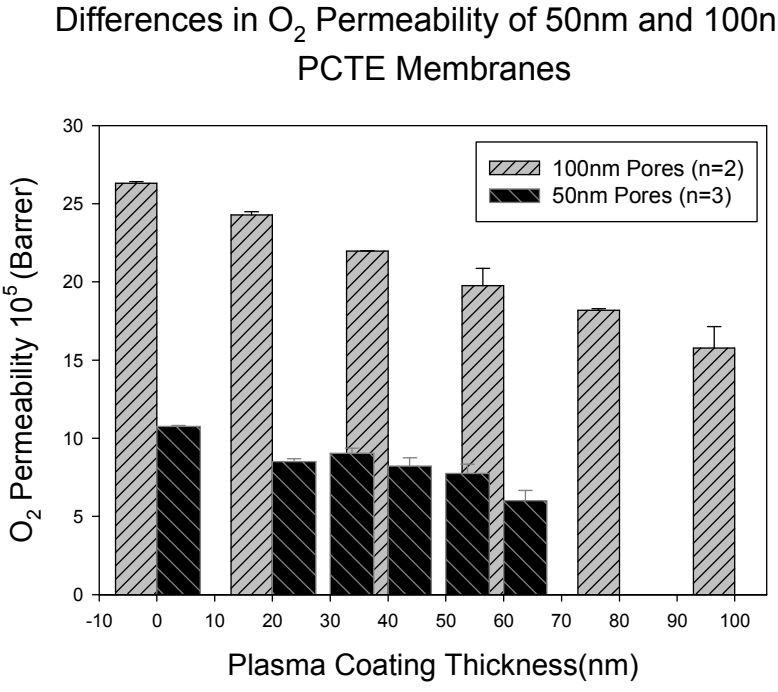

Figure 3.10: Vertical bar plot comparison of O_2 permeability through 50nm and 100nm pore sized PCTE membranes at each C_6F_{14} plasma coating thickness

3.1.5 Effect of Crosslink Density

Samples for this study consisted of 100nm pore-sized PCTE membranes with a 50nm VAA plasma coating. Three coatings each with a different level of crosslink density were produced, each with constant 50nm thickness. It is possible to adjust reaction conditions in the plasma reactor environment in order to vary the crosslink density of the plasma polymerized films. This is primarily due to a relationship between carboxylic acid content and crosslink density. In Figure 3.11 the O_2 permeability is plotted along a series of applied pressures for three different crosslink densities denoted low, medium, and high crosslink density.

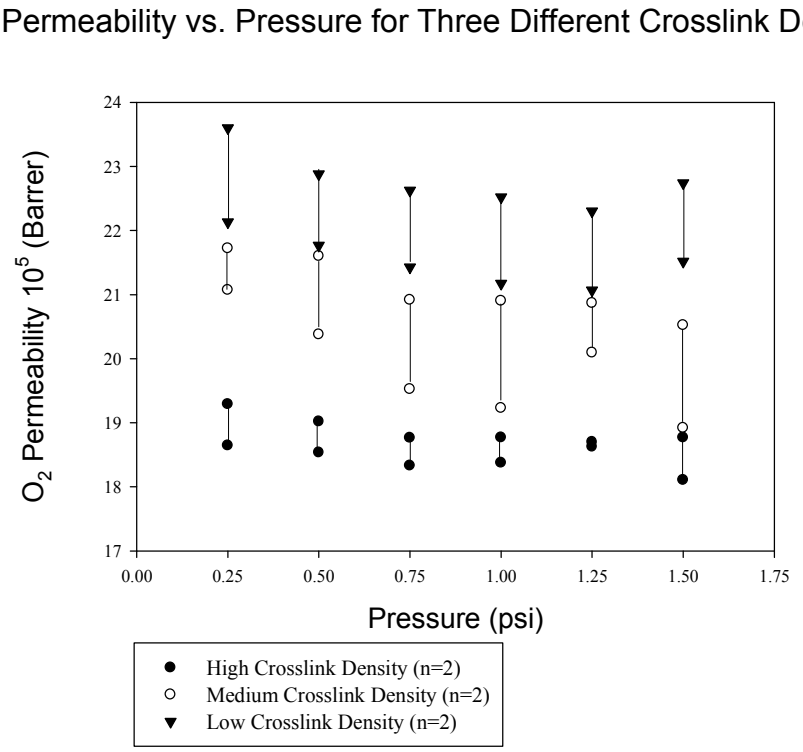

Figure 3.11: O_2 permeability vs. pressure plots for 100nm pore sized PCTE membranes coated with 50nm thick VAA plasma coatings at either low, medium, or high crosslink density

3.1.6 Data Statistics

The flowrate vs. pressure data for all membrane measurements was linearly regressed. The slopes of these regression lines were statistically compared. Firstly, the hypothesis test of equal slopes for all data failed implying that altering the plasma coating thickness causes a significant change in the slope of the flowrate vs. pressure curves, which is proportional to the membrane permeability. Three overall comparisons were made using this hypothesis of equal slopes: 1) The effect of VAA plasma coating thickness on 50nm pore sized PCTE membranes (see Table 3.1), 2) the effect of C_6F_{14} coating thickness on 50nm and 100nm pore sized PCTE membranes (See Table 3.2), and 3) the difference in slope between O_2 and CO_2 permeability through 50nm and 100nm pore sized PCTE membranes plasma coated with C_6F_{14} (See Table. 3.3). In addition, the differences in individual pairs of slopes were compared and found generally to be significantly different as shown in the following tables. Table 3.1 below shows the resulting statistics from comparing the differences of slopes for the two thinnest and the two thickest VAA plasma coatings. Likewise, Table 3.2 shows corresponding results for C_6F_{14} plasma coated PCTE membranes of both 50nm and 100nm pore sizes.

Table 3.1: Statistical Comparison of Slopes of 50nm Pore Sized PCTE Membranes with Different VAA Plasma Coating Thicknesses

Membrane 1	**Membrane 2**					
Coating Thickness, nm	Coating Thickness, nm	Difference in Slope	Std. Error	DF	t value	Pr > |t|
uncoated	10	-99.8909	17.9116	204	-5.58	<0.0001
60	50	-138.93	17.4494	204	-7.96	<0.0001

Table 3.2: Statistical Comparison of Slopes of 50nm and 100nm Pore Sized PCTE Membranes with Different C_6F_{14} Plasma Coating Thicknesses

	Membrane 1	**Membrane 2**					
Membrane Pore Size, nm	Coating Thickness, nm	Coating Thickness, nm	Difference in Slope	Std. Error	DF	t value	Pr > |t|
50	20	Uncoated	-160.30	18.3253	213	-8.75	<0.0001
50	60	50	-96.1325	40.5658	213	-2.37	.0187
100	40	20	-137.23	17.6224	213	-7.79	<0.0001
100	100	80	-132.59	63.5161	213	-2.09	0.0380

The statistical comparison of permeant gases also failed the hypothesis test of equal slopes. This means that the O_2 and CO_2 permeability were significantly different for a given membrane. The difference in slopes for the two gases were also compared at each individual C_6F_{14} coating thickness on both 50nm and 100nm pore sized PCTE membranes. Those results are shown in Table 3.3 below. All membranes except the 20nm coated membranes show a highly significant difference in slopes between O_2 and CO_2 ($P_r < 0.0001$). Also with those two exceptions, the difference in slopes are close to the same for all 50nm pore sized PCTE membranes and the same is true of the 100nm pore sized PCTE membranes. This reinforces the idea that there is a difference of proportion between the O_2 and CO_2 permeability through the PCTE membranes.

Table 3.3: Statistical Comparison of O_2 and CO_2 Slopes of 50nm and 100nm Pore Sized PCTE Membranes with Different C_6F_{14} Plasma Coating Thicknesses

Membrane Pore Size, nm	Coating Thickness, nm	Difference in O_2 and CO_2 Slope	Std. Error	DF	t value	Pr > |t|
100	20	-517.89	233.10	375	-2.22	0.0269
100	40	150.19	12.8041	375	11.73	< 0.0001
100	60	124.58	17.8380	375	6.98	< 0.0001
100	80	122.34	15.1945	375	8.05	< 0.0001
100	100	52.8337	5.5097	375	9.59	< 0.0001
50	20	125.45	67.5347	375	1.86	0.0640
50	30	59.8921	6.0229	375	9.94	< 0.0001
50	40	57.7495	5.3594	375	10.78	< 0.0001
50	50	51.6540	5.5086	375	9.38	< 0.0001
50	60	41.2012	9.7184	375	4.24	< 0.0001

3.2 Contact Angle Measurements of PCTE Membranes

The results of advancing/receding contact angle measurements on multiple PCTE membranes each either uncoated (PVP coated), VAA coated, or C_6F_{14} coated can be seen in Figure 3.12. The relatively constant data points beginning each curve represents the advancing angle, and likewise the second slanted line represents the receding part of the measurements.

A separate set of samples were prepared for a study comparing the contact angles on membranes with varying crosslink density. These samples were coated with VAA at three different crosslink densities. The results from the advancing/receding contact angle measurements are shown in Figure 3.13. To illustrate the concept of water penetration through the pores explicitly, Figure 3.14 shows the water contact angle vs. time for an uncoated 50nm pore-sized PCTE sample.

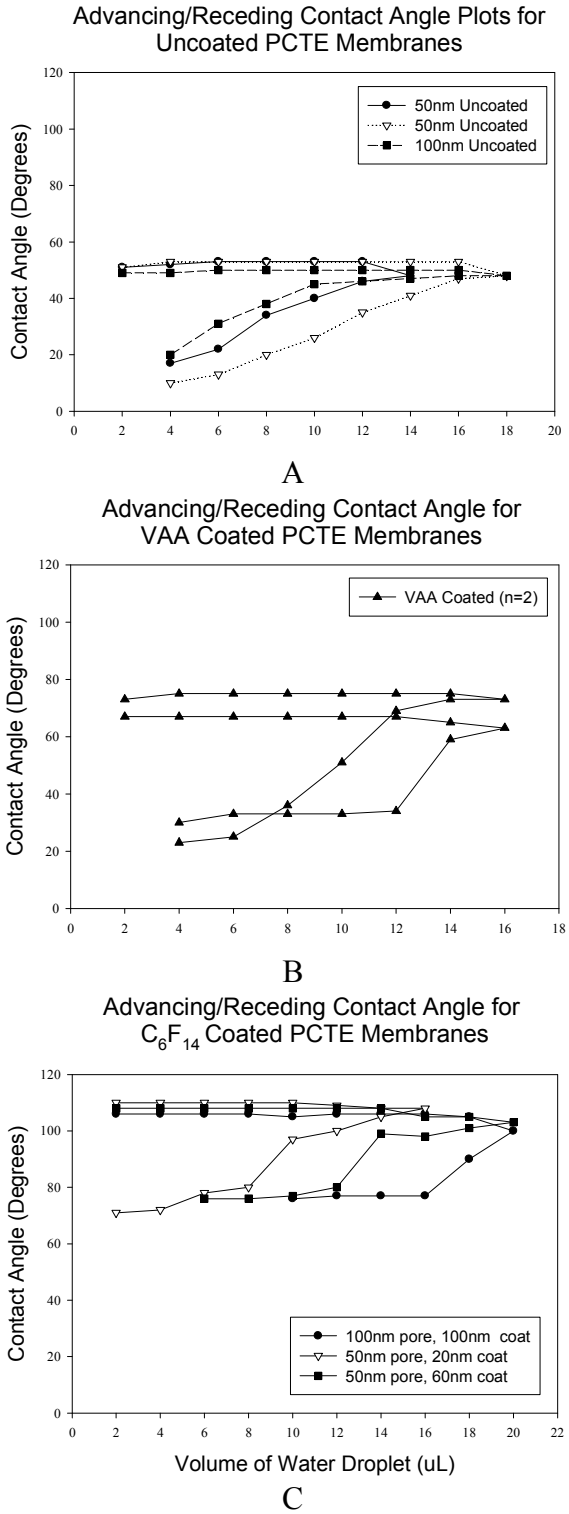

Figure 3.12: Advancing/receding water contact angle vs. water volume plots on PCTE membranes with either A) uncoated (PVP), B) VAA, or C) C_6F_{14} coatings

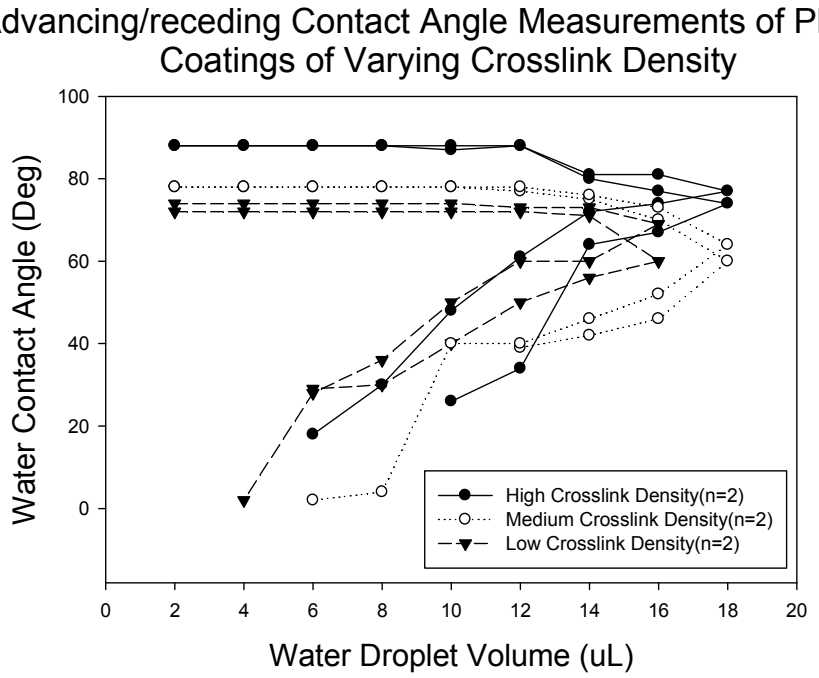

Figure 3.13: Advancing/receding contact angle plots of VAA plasma coated PCTE membranes with three different crosslink densities of the VAA coating

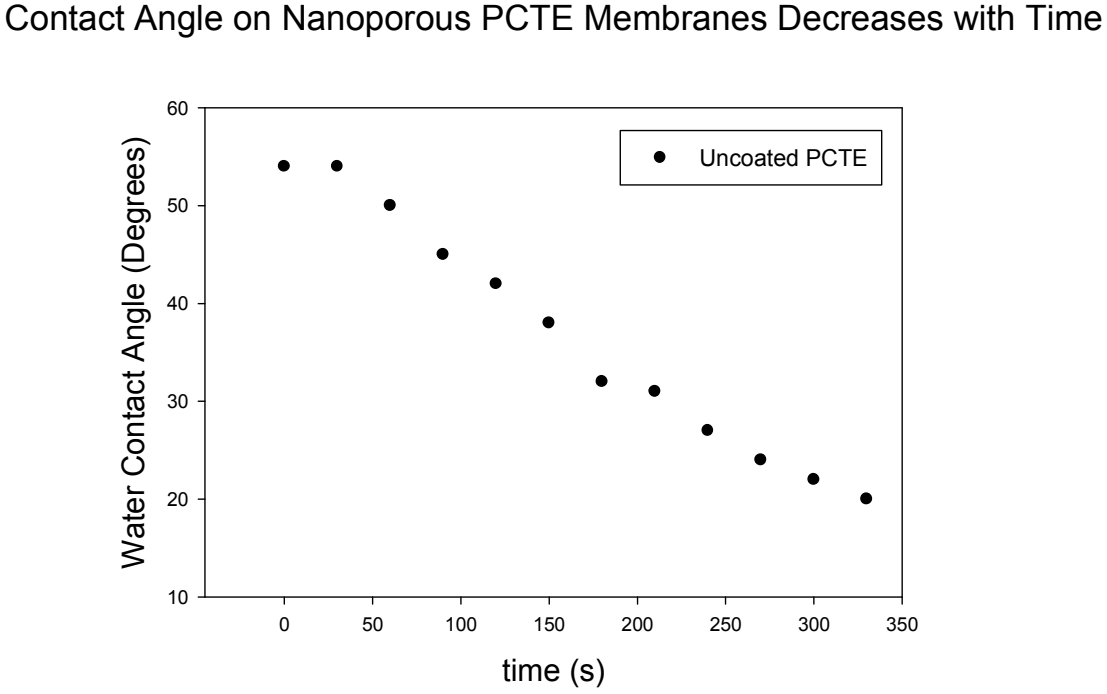

Figure 3.14: Water contact angle vs. time for uncoated 50nm pore sized PCTE membrane

3.3 SEM Photographs of PCTE Membranes

PCTE membranes were examined under SEM for their pore structure. Three photographs in Figure 3.15 show A) PCTE membrane with 50nm pores at 35kx magnification, B) the same membrane at 50kx magnification and a measured pores size of about 50nm, and C) a VAA plasma coated membrane with a measured reduction in pore size of around 30nm. These images clearly show a reduction in pore sizes from uncoated to VAA plasma coated PCTE.

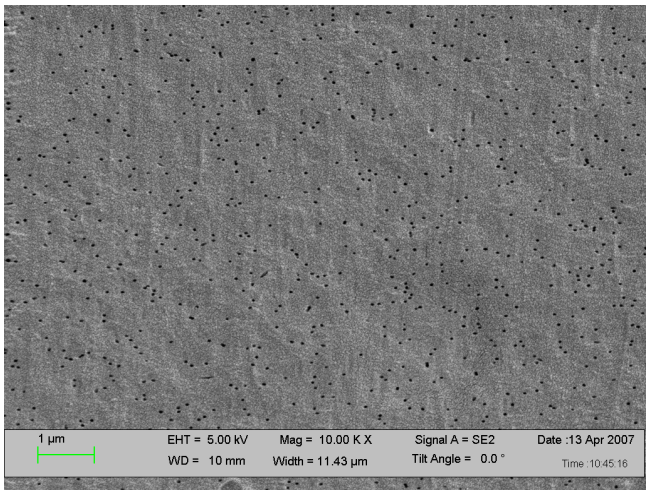

A

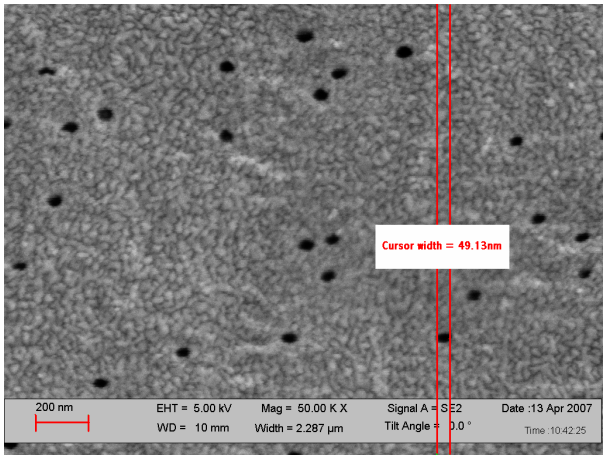

B

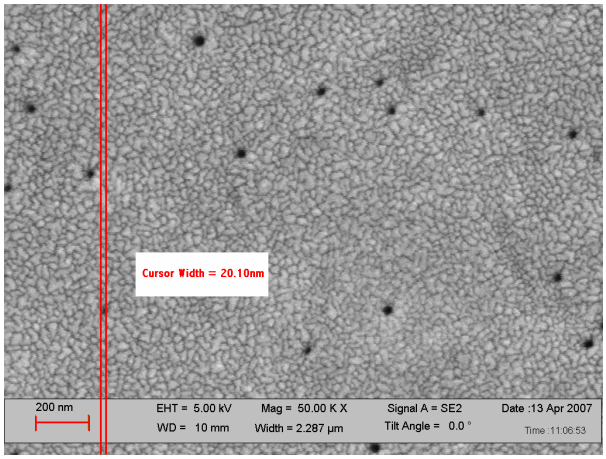

C

Figure 3.15: SEM photographs of PCTE membranes with nominal pore size of 50nm A) at 10kx magnification, B) an uncoated (control) PCTE membrane at 50kx, and C) VAA plasma coated membrane at 50kx.

CHAPTER 4

DISCUSSION

Two main objectives of this study were to measure the gas permeability through and the water contact angle on nanoporous PCTE membranes. A low duty cycle pulsed plasma polymerization technique was implemented to apply a hydrophobic C_6F_{14} or a more hydrophilic VAA coating of varying thickness onto PCTE membranes. The application of the plasma coating served to alter the gas permeability properties of the membrane as well as the wettability of the membrane surface. In order to better understand the effect of plasma coating parameters on permeability and wettability of the membranes, five principal factors affecting the membrane performance were highlighted, namely plasma coating thickness, coating material, permeant gas, membrane pore size, and crosslink density of plasma coating. Three replicates of each sample were studied to demonstrate reproducibility of the plasma treated membranes.

Plasma surface treatments have been applied in many applications including biomaterials, sterilization, reverse osmosis, surface modification, and gas separation. Pulsed plasma polymerization, specifically, has been used to alter the gas permeation properties of polymer substrates as well as alter the wettability surfaces [23, 29-32]. Using this technique, biomolecules can be grafted to the membrane surface to improve biocompatibility. A significant portion of the recent literature has focused on demonstrating good controllability of film chemistry during plasma treatment [21]. It is

known that conditions in plasma reactor environment, such as the duty cycle, can be precisely manipulated in order to create a surface coating that is conformal with a specific thickness. This paper demonstrates this controllability through the altered permeation properties of the PCTE membranes. In short, as the plasma films are grown for longer time, the thicker the coating deposited becomes, resulting in a reduced permeability through the membrane. The feasibility of this technique is presently demonstrated on PCTE membranes and is intended to be applied to modify nanoporous silicon nitride membranes. These silicon nitride membranes will be part of a series of microfabricated nanoporous microchannels combined to form a novel blood oxygenator device.

4.1 Effect of Coating Thickness

Authors have shown that plasma treatment can be used to alter the pore characteristics in porous substrates by increasing plasma deposition times to adjust coating thickness [24, 33-36]. Another group has recently grafted PNIPAm to nanoporous PCTE membranes and demonstrated a gradual reduction in pore size directly resulting in a gradual reduction in water permeability through the porous membrane [37, 38]. The concept of coating the pore walls gradually narrowing the pores is not new, however. It has been verified by AFM that pulsed plasma treatment will reduce the pore size by coating the pore walls on 200nm PCTE membranes [25]. Yamammoto and others report that a coating thickness of five times the pore radius is typically needed to completely clog the pores [34] and clogging the pores is typically essential to cause permselectivity of gases through the membrane. In another similar

study the authors used the same approach on siloxane-type plasma coated Polypropylene membranes [35, 39] and although the substrates and plasma coatings were of different materials, the same magnitude of permeability values were observed in the present study, some of the highest permeability values recorded for any polymer. It is known that siloxane-type materials have some of the highest O_2 and CO_2 permeability characteristics of any polymer. Consequently, siloxane coatings are currently applied to blood oxygenator membranes to improve compatibility and performance.

Tables of data are available on gas permeability through many polymers [3, 5, 7, 40]. Gas permeability values reported in the aforementioned studies by other investigators ranged from 10 Barrers up to around $2x10^6$ Barrers depending on the film and substrate under study. In the present study permeability values ranged from about $1x10^5$ to $2x10^6$ Barrers depending on the membrane pore size and the thickness of plasma coating although there should be no reason that an even wider range could be achieved with even thicker coatings and other pore sizes.

In the past, gas permeation measurements were commonly used as a means of determining mean pore size of a material [41]. However, in the case of the PCTE membranes under study the details of the pore sizes are already known. This allows the investigator to consider methods traditionally used to characterize nonporous membranes to characterize porous membranes. Table 4.1 lists some important characteristics of the commercially available PCTE membranes [14].

Table 4.1: Properties of Sterlitech Nanoporous PCTE Membranes

Pore Size (nm)	Pore Density (pores/cm^2)	Nominal Thickness (um)
50	6e8 ± 9e7	6 ± 0.6
100	4e8 ± 6e7	6 ± 0.6

Pulsed plasma polymerization of films with different thicknesses was applied to enable one to prescribe specific permeability ranges to the porous substrate. Sakata, Yamamoto, and Hirai indicate that "In the course of the deposition process, reduction of pore size, gradual clogging of pores and formation of homogeneous pinhole-free films" can be achieved using this approach [34]. When applying very thin films, however, say in the 10nm-20nm range, it can be difficult to precisely control the deposition. This could be the reason a significant difference in gas flux can be seen with plasma coatings 30nm or higher whereas the thinner coatings do show noticeable, but not significant, differences (see Figure 3.2). Some evidence of the pore reduction concept has been presented in this study through SEM photographs. The photographs show a definite reduction in pore size of up to 60% as a result of plasma coating.

4.2 Coating Material

VAA and C_6F_{14} were used as plasma coating materials. These coatings, along with many others, have been used previously in pulsed plasma polymerization [26, 42]. There was a noticeable but not significant trend. As coating thickness increased, VAA coated membranes first resulted in higher permeability than C_6F_{14}. As the thicker coating thicknesses are approached the opposite is true: C_6F_{14} coated membranes become more permeable than VAA coated membranes. Also, this difference increases

as coating thickness increases. The effects of the different coating materials on PCTE membranes are also illustrated through the contact angle experiments.

The purchased PCTE membranes are denoted "uncoated" although a hydrophilic PVP wetting agent was applied by the manufacturer. As a result, contact angle measurements should indicate a hydrophilic surface. This was in fact the case. .

The uncoated contact angle was measured to be around 53^0 and the contact angle for the VAA and C_6F_{14} coated samples were around 73^0 and 105^0, respectively. C_6F_{14} successfully altered the membrane surface from hydrophilic to hydrophobic. This is the reason C_6F_{14} was chosen as a polymer for surface treatment, its hydrophobic nature. De Gennes [8, 9] reported that advancing/receding contact angle measurements on nanoporous membranes is not very informative since water will immediately penetrate the pores. This is true in some cases, but in the current study after careful comparison of the advancing/receding contact angle plots, an important trend is seen. A simple contact angle vs. time experiment nicely demonstrated the penetration of water through the pores. As the receding angle plot illustrates, water penetrated the pores in all samples; however, the more hydrophobic the coating, the less water penetrates the pores. In other words, upon receding, the contact angle of the C_6F_{14} samples only dropped to around 70^0 while the other samples dropped below 20^0.

4.3 Permeant Gas

Two different low molecular weight gases, O_2 and CO_2, were used as permeant gases for the permeability studies. With a specific application in mind, membranes for blood oxygenators, the author was interested in characterizing the permeability of O_2

and CO_2 specifically, through the PCTE membranes. For gas separation applications however, an emphasis is placed on the relative permeability of one permeant gas over another. Typically, when dealing with porous materials, it is helpful to first calculate the Knudsen number *Kn* to determine the flow regime. In this case, for *Kn*=0.116 it is expected that the flow lie in the transition regime since *Kn* is neither extremely smaller than one nor extremely larger than one. If Knudsen flow dominates then the gas permeability through the PCTE membranes should be proportional to $\left(\sqrt{M}\right)^{-1}$. It was immediately noticed that O_2 was more permeable than the CO_2. A plot of O_2 permeability vs. CO_2 permeability from all C_6F_{14} treated samples, including all coating thicknesses and both 50nm and 100nm pore sized membranes, was linearly regressed (r^2=0.9958) and the slope was calculated to be approximately 1.12. When only considering the 50nm pore-sized PCTE data points, a ratio of 1.167 was calculated from the linear trendline in accordance with a Dalton's law-type dependence on the ratio of the square roots of molecular weight for CO_2 and O_2, namely:

$$\frac{\sqrt{44}}{\sqrt{32}} = 1.172 .$$

This close agreement suggests that the transport through the PCTE membranes may be dominated by Knudsen-type flow although this should be verified through more permeability studies using more permeant gases. This dependence on Knudsen flow is also more pronounced in the 50nm as opposed to the 100nm pore sized PCTE membranes. An important physiological note is that the ration of O_2 and CO_2 regarding human metabolism is around 1.2.

4.4 Membrane Pore Size

PCTE membranes with 50nm and 100nm pores were chosen for this study. Both were, of course, plasma coated to varying degrees as before. Table 4.1 lists the pore density for the PCTE membranes. The ratio of pore densities for the 50nm and 100nm pore-sized PCTE is:

$$\frac{6x10^{8}\ pores/cm^{2}}{4x10^{8}\ pores/cm^{2}} = 1.5$$

But remember, the surface area of each of the 100nm pores is 4 times larger than the 50nm pores. The end result is, assuming the gas flow through both pore sizes follows the same type of transport, then the PCTE with 100nm pores should have a flux roughly 8/3 higher than the 50nm pores. Results agreed within the range of tolerances. Again, it remains unclear though, the extent of Knudsen flow behavior for both cases.

The permeability through PCTE membranes, as plasma coating thickness increased, behaved differently for the two membrane pore sizes. For the PCTE with 50nm pores, the permeability vs. coating thickness plot was fitted to a second order polynomial whereas the same plot in the 100nm case seemed to indicate a linear trend. This nonlinearity could simply be the result of a non-uniform coating at the lower coating thicknesses or it could mean that the pores were not all coated equally. Sae-Joong et al applied 0.1 to 1um thick plasma coatings and also reported a linear correlation between plasma coating thickness and permeability [43]. This again was the case in the present study only for the PCTE membranes with 100nm pores. In addition,

it was also noticed that for the 100nm PCTE, the permeability change was minimal when the coating thickness approached the pore diameter.

4.5 Effect of Crosslink Density

Reactor conditions were manipulated in order to coat low, medium, and high crosslink density polymer films onto PCTE membranes. A 50nm thick VAA-coated sample set was compared for gas permeability studies and samples from both 50nm and 80nm VAA coated PCTE membranes were used for contact angle measurements. Results indicated a decrease in permeability for both gases as crosslink density was increased. The permeability measured from 0.25psi to 1.75psi yielded three distinct ranges of values corresponding to the level of crosslink density. The permeability values ranged from 1.8×10^6 Barrers, at high crosslink density, to 2.3×10^6 Barrers, at low crosslink density. The author suggests it may be possible to custom-tailor the permeability in two steps, first by applying a specific thickness of coating, and secondly, by applying that coating with a specific level of crosslink density. It was also recognized that the contact angle increased by around 10^0 as crosslink density increased, demonstrating a more hydrophobic surface.

CHAPTER 5

CONCLUSION

As membranes have become important components in many mass transfer applications, an interest has been dedicated to finding the best materials for the intended application. To contribute to this, the current study has aimed to demonstrate the feasibility of modifying nanoporous PCTE membranes via the low duty cycle pulsed plasma polymerization of thin films with the purpose of modulating the gas permeability through the membranes. As was shown, these films have important consequences on the wettability of the membrane surface as well. Aspects such as plasma coating thickness, coating material, permeant gas, membrane pore size, and crosslink density were shown to affect gas permeability and water contact angle on modified PCTE membranes.

Blood oxygenation is an intended future application of this process. It was shown that the modified PCTE membranes had sufficient O_2 and CO_2 transfer for this purpose. In addition to this, the C_6F_{14}-modified membranes demonstrated hydrophobic properties suitable for oxygenator applications.

CHAPTER 6

FUTURE WORK

An important goal for future work will focus on characterizing the morphology of the coated pore cross-section, to gain insight into the consistency of the plasma coating along the pore walls. This can be done by cutting or fracturing the membranes along a cross-section and viewing under SEM. In addition to this, it will be helpful to develop a correlation between plasma reactor conditions and permeability of a certain gas through the membrane. Two important pieces of information that need to be elucidated are: 1) at what plasma coating thickness do the pores become completely clogged and 2) if very thin coatings are applied, say in 5-10nm range, does partial coating occur? As a result, how do these affect the permeability and permselectivity of the membranes? Future studies will involve applying this process to membranes for blood oxygenator devices, particularly to microfabricated silicon nitride nanoporous microchannels.

APPENDIX A

EXPERIMENTAL LEGEND

SUMMARY OF ALL MEMBRANE EXPERIMENTS					
Exp #	Pore size,nm	Name,Coat thickness,nm	Gases 1,2	ΔP, psi	Coat Material
23	50	U5 (40nm)	1	0.25-4	VAA
24	50	U4 (30nm)	1	0.25-4	VAA
25	50	P2 (20nm)	1	0.25-4.5	VAA
26	50	U6 (Blank)	1	0.25-3.5	VAA
27	50	U6 rerun	1		VAA
28	50	U7 (Blank)	1	0.25-3.25	VAA
29	50	U3 (10nm)	1	0.25-2.75	VAA
30	50	U2 (20nm)	1	0.25-3.25	VAA
31	50	U1 (30nm)	1	0.25-4	VAA
32	50	U8 (Blank)	1	0.1-1,0.25-2.5	VAA
33	50	U9 (Blank)	1	0.1-1,0.25-3	VAA
34	50	U10 (Blank)	1	0.1-1,0.25-3	VAA
35	50	60A	1	0.1-3	VAA
36	50	50A	1	0.1-3	VAA
37	50	40A	1	0.1-3	VAA
38	50	30A	1	0.1-3	VAA
39	50	20A	1	0.1-3	VAA
40	50	10A	1	0.1-3	VAA
41	50	60B	1	0.1-3	VAA
42	50	50B	1	0.1-3	VAA
43	50	40B	1	0.1-3	VAA
44	50	30B	1	0.1-3	VAA
45	50	20B	1	0.1-3	VAA
46	50	10B	1	0.1-3	VAA
47	100	Blank	1	0.1-3	VAA
48	50	60C	2	0.25-2.5	VAA
49	50	60A	2,1	0.25-2.5	C6F14
50	100	60A	1,2	0.25-2.5	C6F14
51	50	50C	2,1	0.25-2.5	VAA
52	50	40C	1,2	0.25-2.5	VAA
53	100	100A	2,1	0.25-2.5	C6F14

SUMMARY OF ALL MEMBRANE EXPERIMENTS					
Exp #	**Pore size,nm**	**Name,Coat thickness,nm**	**Gases 1,2**	**ΔP, psi**	**Coat Material**
54	100	80A	1,2	0.25-2.5	C6F14
55	100	40A	2,1	0.25-2.5	C6F14
56	100	20A	1,2	0.25-	C6F14
57	50	50A	2,1	0.25-	C6F14
58	50	40A	1,2	0.25-	C6F14
59	50	30A	2,1	0.25-	C6F14
60	50	20A	1,2	0.25-2.25	C6F14
61	50	30C	1,2	0.25-2.5	VAA
62	50	20C	1,2	0.25-2.5	VAA
63	50	10C	1,2	0.25-2.25	VAA
64	50	20B	1,2	0.25-2.5	C6F14
65	50	30B	1,2	0.25-2.5	C6F14
66	50	40B	1,2	0.25-2.5	C6F14
67	50	50B	1,2	0.25-2.5	C6F14
68	50	60B	1,2	0.25-2.5	C6F14
69	100	50A-L	1,2	0.25-1.5	VAA
70	100	50A-M	1,2	0.25-1.5	VAA
71	100	50A-H	1,2	0.25-2.0	VAA
72	100	20B	1,2	0.25-1.75	C6F14
73	100	40B	1,2	0.25-1.5	C6F14
74	100	60B	1,2	0.25-1.75	C6F14
75	100	80B	1,2	0.25-1.75	C6F14
76	100	100B	1,2	0.25-1.75	C6F14
77	100	50B-L	1,2	0.25-1.75	VAA
78	100	50B-M	1,2	0.25-1.75	VAA
79	100	50B-H	1,2	0.25-1.75	VAA
80	50	50-60C	1,2	0.25-2.5	C6F14
81	50	50-50C	1,2	0.2-2.5	C6F14
82	50	50-40C	1,2	0.25-2.5	C6F14
83	50	50-30C	1,2	0.25-2.5	C6F14
84	50	50-20C	1,2	0.25-2.5	C6F14

APPENDIX B

RAW FLOWRATE DATA

B.1 RAW FLOWRATE DATA FOR UNCOATED PCTE

RAW PERMEABILITY DATA FOR UNTREATED PCTE					
Exp. #	Pore size,nm	Coating thickness,nm	P (psi)	Flow rate	Permeability (Barrer)
26	50	0	0.25	162	1229228
26	50	0	0.5	306	1161080
26	50	0	0.75	461	1167627
26	50	0	1	612	1163107
26	50	0	1.25	772	1173877
26	50	0	1.5	943	1193680
26	50	0	1.75	1088	1180816
26	50	0	2	1226	1164554
26	50	0	2.25	1386	1170005
26	50	0	2.5	1501	1140409
26	50	0	2.75	1616	1116010
26	50	0	3	1821	1152859
26	50	0	3.25	1957	1143915
27	50	0	0.5	299	1135292
27	50	0	1	594	1128105
27	50	0	1.5	906	1147032
27	50	0	2	1190	1129897
27	50	0	2.5	1482	1126380
27	50	0	3	1758	1113132
27	50	0	3.5	2061	1118409
28	50	0	0.25	154	1168444
28	50	0	0.5	299	1134501
28	50	0	0.75	446	1129274
28	50	0	1	567	1076761

28	50	0	1.25	707	1074555
28	50	0	1.5	844	1069366
28	50	0	1.75	986	1069881
28	50	0	2	1129	1072129
28	50	0	2.25	1259	1063384
28	50	0	2.5	1476	1121407
28	50	0	2.75	1562	1078863
28	50	0	3	1711	1083741
28	50	0	3.25	1830	1069974
32	50	0	0.25	141	1070789
32	50	0	0.5	282	1071272
32	50	0	0.75	431	1070100
32	50	0	1	560	1064073
32	50	0	1.25	696	1058351
32	50	0	1.5	841	1065509
32	50	0	1.75	993	1077692
32	50	0	2	1146	1088464
32	50	0	2.25	1294	1092272
32	50	0	2.5	1422	1080922
33	50	0	0.25	140	1060325
33	50	0	0.5	293	1114315
33	50	0	0.75	439	1111444
33	50	0	1	587	1114644
33	50	0	1.25	730	1110148
33	50	0	1.5	883	1117825
33	50	0	1.75	975	1058763
33	50	0	2	1117	1060914
33	50	0	2.25	1269	1071036
33	50	0	2.5	1409	1070825
33	50	0	2.75	1484	1025459
34	50	0	0.25	144	1096573
34	50	0	0.5	280	1063083

34	50	0	0.75	414	1048411
34	50	0	1	556	1056200
34	50	0	1.25	701	1065282
34	50	0	1.5	848	1073611
34	50	0	1.75	986	1070230
34	50	0	2	1122	1066090
34	50	0	2.25	1290	1089483
34	50	0	2.5	1429	1085571

B.2 RAW FLOWRATE DATA FOR C6F14-COATED PCTE

RAW C6F14-COATED PCTE PERMEABILITY DATA

Exp. #	Pore size,nm	Name	Coating thickness,nm	P (psi)	O2 Flow rate	O2 Permeability (Barrer)	CO2 Flow rate	CO2 Permeability (Barrer)
53	100	100-100A	100	0.25	193	1464160	222	1687460
53	100	100-100A	100	0.5	376	1429086	430	1634176
53	100	100-100A	100	0.75	562	1422485	616	1560668
53	100	100-100A	100	1	750	1424154	788	1497824
53	100	100-100A	100	1.25	935	1420383	954	1449817
53	100	100-100A	100	1.5	1118	1415687	1098	1390740
53	100	100-100A	100	1.75	1306	1417254	1260	1367336
53	100	100-100A	100	2	1493	1418532	1417	1345577
53	100	100-100A	100	2.25	1644	1388184	1610	1359654
54	100	100-80A	80	0.25	241	1827862	221	1679204
54	100	100-80A	80	0.5	491	1863785	437	1662050
54	100	100-80A	80	0.75	741	1877311	648	1642298
54	100	100-80A	80	1	967	1837261	853	1620494
54	100	100-80A	80	1.25	1211	1840152	1084	1647183
54	100	100-80A	80	1.5	1427	1806989	1314	1663802
54	100	100-80A	80	1.75	1708	1853706	1471	1597276
54	100	100-80A	80	2	1905	1809452	1615	1533754
50	100	100-60A	60	0.25	282	2146174	272	2065460
50	100	100-60A	60	0.5	559	2123792	511	1940809
50	100	100-60A	60	0.75	833	2110321	750	1899749
50	100	100-60A	60	1	1121	2129782	988	1876609
50	100	100-60A	60	1.25	1449	2202832	1233	1874160
50	100	100-60A	60	1.5	1650	2090260	1466	1856157

50	100	100-60A	60	1.75	1911	2074516	1686	1829794
55	100	100-40A	40	0.25	288	2191807	282	2142945
55	100	100-40A	40	0.5	579	2201312	548	2081192
55	100	100-40A	40	0.75	851	2155729	820	2078168
55	100	100-40A	40	1	1186	2253805	1034	1963965
55	100	100-40A	40	1.25	1453	2208029	1340	2036930
55	100	100-40A	40	1.5	1709	2163812	1547	1958948
56	100	100-20a	20	0.1	147	2794457	119	2254504
56	100	100-20a	20	0.2	281	2664928	234	2219999
56	100	100-20a	20	0.3	418	2645200	346	2193981
56	100	100-20a	20	0.4	538	2557401	467	2215870
56	100	100-20a	20	0.5	667	2532970	578	2197909
56	100	100-20a	20	0.6	795	2517604	584	1849821
56	100	100-20a	20	0.7	919	2493678	817	2217846
56	100	100-20a	20	0.8	1039	2467659	927	2200134
56	100	100-20a	20	0.9	1146	2417951	1028	2170947
56	100	100-20a	20	1	1275	2422207	1156	2196377
56	100	100-20a	20	1.1	1393	2406520	1342	2317451
49	50	50-60A	60	0.25	78	594285	74	565399
49	50	50-60A	60	0.5	153	580964	143	544106
49	50	50-60A	60	0.75	227	575500	216	546330
49	50	50-60A	60	1	303	574802	286	542571
49	50	50-60A	60	1.25	376	571419	354	538296
49	50	50-60A	60	1.5	452	572983	423	535284
49	50	50-60A	60	1.75	526	571351	487	528168
49	50	50-60A	60	2	603	572441	550	522584
49	50	50-60A	60	2.25	677	571667	613	517358
49	50	50-60A	60	2.5			670	509431
57	50	50-50A	50	0.25	89	676096	81	615491
57	50	50-50A	50	0.5	179	680845	158	602136
57	50	50-50A	50	0.75	259	655416	238	603661
57	50	50-50A	50	1	344	653152	314	596086
57	50	50-50A	50	1.25	431	654515	390	592813
57	50	50-50A	50	1.5	517	654531	469	594501
57	50	50-50A	50	1.75	603	654347	545	591478
57	50	50-50A	50	2	687	652580	621	589616
57	50	50-50A	50	2.25	777	656227	704	594733
57	50	50-50A	50	2.5			800	607593
57	50	50-50A	50	2.75			873	603356
58	50	50-40A	40	0.25	119	907527	104	790792
58	50	50-40A	40	0.5	242	918927	209	793366
58	50	50-40A	40	0.75	343	868944	327	827468
58	50	50-40A	40	1	467	886711	434	823938

58	50	50-40A	40	1.25	580	881550	541	822256
58	50	50-40A	40	1.5	697	882172	619	784377
58	50	50-40A	40	1.75	816	885713	732	794906
58	50	50-40A	40	2	919	873067	836	794443
58	50	50-40A	40	2.25	1063	897465	860	726414
59	50	50-30A	30	0.25	110	836914	103	785163
59	50	50-30A	30	0.5	221	840525	201	764493
59	50	50-30A	30	0.75	332	841795	305	772757
59	50	50-30A	30	1	445	845824	407	774034
59	50	50-30A	30	1.25	557	847146	505	767832
59	50	50-30A	30	1.5	664	840585	601	761262
59	50	50-30A	30	1.75	772	838328	693	752828
59	50	50-30A	30	2	887	842832	785	745602
59	50	50-30A	30	2.25	995	839852	886	747663
60	50	50-20A	20	0.25	104	788569	86	654174
60	50	50-20A	20	0.5	196	744046	165	625679
60	50	50-20A	20	0.75	290	734194	250	634035
60	50	50-20A	20	1	381	724720	332	630788
60	50	50-20A	20	1.25	477	724176	416	632455
60	50	50-20A	20	1.5	568	719057	495	626767
60	50	50-20A	20	1.75	658	713896	578	627020
60	50	50-20A	20	2	749	711210	652	619479
60	50	50-20A	20	2.25	852	719389	744	627763
64	50	50-20B	20	0.25	121	917410	98	744037
64	50	50-20B	20	0.50	228	866814	210	797769
64	50	50-20B	20	0.75	336	850766	296	749700
64	50	50-20B	20	1.00	447	848599	393	746372
64	50	50-20B	20	1.25	555	843081	488	741737
64	50	50-20B	20	1.50	663	840214	593	750607
64	50	50-20B	20	1.75	763	828137	700	759711
64	50	50-20B	20	2.00	873	829419	794	754528
64	50	50-20B	20	2.25	983	830257	911	769012
64	50	50-20B	20	2.50	1099	835082	0	0
65	50	50-30B	30	0.25	124	943351	114	869188
65	50	50-30B	30	0.50	252	956085	222	843845
65	50	50-30B	30	0.75	369	933762	332	840679
65	50	50-30B	30	1.00	491	932761	437	830783
65	50	50-30B	30	1.25	618	939529	546	829424
65	50	50-30B	30	1.50	734	930100	652	825791
65	50	50-30B	30	1.75	877	951763	754	818264
65	50	50-30B	30	2.00	993	943318	861	817718
65	50	50-30B	30	2.25	1118	944174	962	812126
65	50	50-30B	30	2.50	1262	958669	1093	830797

66	50	50-40B	40	0.25	131	992663	111	845908
66	50	50-40B	40	0.50	240	913490	218	827559
66	50	50-40B	40	0.75	359	908529	318	804881
66	50	50-40B	40	1.00	475	902486	422	802590
66	50	50-40B	40	1.25	593	901428	526	798906
66	50	50-40B	40	1.50	715	905503	615	778580
66	50	50-40B	40	1.75	835	906658	721	782907
66	50	50-40B	40	2.00	945	897508	826	784578
66	50	50-40B	40	2.25	1052	887906	929	783965
66	50	50-40B	40	2.50	1172	890887	1056	802720
67	50	50-50B	50	0.25	111	844361	102	773050
67	50	50-50B	50	0.50	219	830914	193	734194
67	50	50-50B	50	0.75	325	822593	292	739335
67	50	50-50B	50	1.00	436	827767	386	733861
67	50	50-50B	50	1.25	535	813256	481	731019
67	50	50-50B	50	1.50	647	819914	569	720685
67	50	50-50B	50	1.75	755	819299	665	721948
67	50	50-50B	50	2.00	858	814872	756	717782
67	50	50-50B	50	2.25	966	815794	857	723733
67	50	50-50B	50	2.50	1100	835662	941	715111
68	50	50-60B	60	0.25	67	512430	60	459547
68	50	50-60B	60	0.50	134	508534	130	492412
68	50	50-60B	60	0.75	200	507404	189	478944
68	50	50-60B	60	1.00	265	503774	248	471683
68	50	50-60B	60	1.25	331	503517	306	465192
68	50	50-60B	60	1.50	397	503240	359	454208
68	50	50-60B	60	1.75	464	503505	420	455925
68	50	50-60B	60	2.00	525	499143	479	455425
68	50	50-60B	60	2.25	588	496757	537	453535
68	50	50-60B	60	2.50	659	500476	591	448755
69	100	100-50A-L	50	0.25	291	2212872	286	2172759
69	100	100-50A-L	50	0.50	573	2176518	566	2151853
69	100	100-50A-L	50	0.75	846	2142509	846	2142356
69	100	100-50A-L	50	1.00	1114	2117112	1100	2089998
69	100	100-50A-L	50	1.25	1386	2106967	1348	2048337
69	100	100-50A-L	50	1.50	1699	2151502	1650	2090105
70	100	100-50A-M	50	0.25	277	2107125	278	2111501
70	100	100-50A-M	50	0.50	536	2037603	539	2046048
70	100	100-50A-M	50	0.75	771	1952505	811	2053791
70	100	100-50A-M	50	1.00	1012	1922857	1077	2045817

70	100	100-50A-M	50	1.25	1322	2009529	1311	1992480
70	100	100-50A-M	50	1.50	1494	1891730	1544	1955562
70	100	100-50A-M	50	1.75	1648	1788486		
71	100	100-50A-H	50	0.25	254	1929195	216	1645071
71	100	100-50A-H	50	0.50	501	1901629	452	1718979
71	100	100-50A-H	50	0.75	741	1876273	687	1740115
71	100	100-50A-H	50	1.00	988	1876645	908	1724550
71	100	100-50A-H	50	1.25	1226	1862531	1130	1717965
71	100	100-50A-H	50	1.50	1430	1810644	1323	1676129
71	100	100-50A-H	50	1.75	1707	1853293	1501	1629269
71	100	100-50A-H	50	2.00			1723	1636914
72	100	100-20B	20	0.25	331	2513715	291	2211755
72	100	100-20B	20	0.50	636	2417001	585	2222771
72	100	100-20B	20	0.75	947	2397906	869	2200056
72	100	100-20B	20	1.00	1267	2406926	1117	2122674
72	100	100-20B	20	1.25	1599	2429928	1366	2076426
72	100	100-20B	20	1.50	1876	2375329	1599	2024807
72	100	100-20B	20	1.75	0	0	1859	2018555
73	100	100-40B	40	0.25	304	2307348	287	2177314
73	100	100-40B	40	0.50	595	2259332	543	2061619
73	100	100-40B	40	0.75	876	2219987	791	2002916
73	100	100-40B	40	1.00	1184	2248339	1029	1955226
73	100	100-40B	40	1.25	1467	2229692	1273	1935421
73	100	100-40B	40	1.50	1693	2144548	1479	1872729
74	100	100-60B	60	0.25	247	1875814	227	1724950
74	100	100-60B	60	0.50	494	1877506	458	1741006
74	100	100-60B	60	0.75	728	1843957	678	1718452
74	100	100-60B	60	1.00	964	1831421	907	1722989
74	100	100-60B	60	1.25	1199	1821581	1141	1734335
74	100	100-60B	60	1.50	1439	1822629	1283	1625106
74	100	100-60B	60	1.75	1710	1856381	1539	1670536
75	100	100-80B	80	0.25	255	1935069	227	1728489
75	100	100-80B	80	0.50	488	1854346	440	1671314

75	100	100-80B	80	0.75	719	1820100	656	1660969
75	100	100-80B	80	1.00	952	1808180	862	1637782
75	100	100-80B	80	1.25	1197	1819452	1091	1658637
75	100	100-80B	80	1.50	1459	1848173	1325	1677545
75	100	100-80B	80	1.75	1621	1759495	1450	1574418
76	100	100-100B	100	0.25	241	1829592	220	1675516
76	100	100-100B	100	0.50	470	1784617	429	1631831
76	100	100-100B	100	0.75	698	1768458	639	1619210
76	100	100-100B	100	1.00	921	1750364	827	1571057
76	100	100-100B	100	1.25	1147	1743592	1037	1576043
76	100	100-100B	100	1.50	1372	1737393	1263	1599210
76	100	100-100B	100	1.75	1598	1734968	1430	1552498
77	100	100-50B-L	100	0.25	311	2359946	282	2146244
77	100	100-50B-L	100	0.50	602	2287915	555	2107313
77	100	100-50B-L	100	0.75	893	2262469	811	2055440
77	100	100-50B-L	100	1.00	1185	2251839	1058	2010697
77	100	100-50B-L	100	1.25	1467	2229887	1347	2047620
77	100	100-50B-L	100	1.50	1795	2273926	1611	2040493
78	100	100-50B-M	100	0.25	286	2172354	267	2031262
78	100	100-50B-M	100	0.50	569	2160023	512	1944776
78	100	100-50B-M	100	0.75	826	2091680	752	1905455
78	100	100-50B-M	100	1.00	1100	2090360	998	1895969
78	100	100-50B-M	100	1.25	1373	2086939	1239	1883463
78	100	100-50B-M	100	1.50	1620	2052231	1507	1908048
79	100	100-50B-H	100	0.25	245	1864307	224	1702436
79	100	100-50B-H	100	0.50	488	1853407	438	1664238
79	100	100-50B-H	100	0.75	724	1832838	642	1626841
79	100	100-50B-H	100	1.00	967	1837288	842	1599540
79	100	100-50B-H	100	1.25	1230	1869711	1042	1583731
79	100	100-50B-H	100	1.50	1482	1876733	1235	1564359
80	50	50-60C	60	0.25	97	739204	89	674276
80	50	50-60C	60	0.50	187	709995	173	657455

80	50	50-60C	60	0.75	282	713311	257	649978
80	50	50-60C	60	1.00	377	715796	339	643628
80	50	50-60C	60	1.25	468	711400	422	640987
80	50	50-60C	60	1.50	566	716488	503	636849
80	50	50-60C	60	1.75	669	726144	583	633225
80	50	50-60C	60	2.00	775	735956	663	629885
80	50	50-60C	60	2.25	859	725166	737	621893
80	50	50-60C	60	2.50	962	730900	820	623385
81	50	50-50C	50	0.25	110	837837	103	784302
81	50	50-50C	50	0.50	225	856704	201	762988
81	50	50-50C	50	0.75	338	856408	303	767022
81	50	50-50C	50	1.00	450	854329	402	763145
81	50	50-50C	50	1.25	562	854779	495	752737
81	50	50-50C	50	1.50	671	849806	593	750881
81	50	50-50C	50	1.75	782	848539	688	747123
81	50	50-50C	50	2.00	883	838914	783	743693
81	50	50-50C	50	2.25	996	840689	889	750512
81	50	50-50C	50	2.50	1109	842603	968	735630
82	50	50-40C	40	0.25	119	906097	110	833362
82	50	50-40C	40	0.50	234	887204	206	782493
82	50	50-40C	40	0.75	343	868356	306	774764
82	50	50-40C	40	1.00	454	862596	403	765519
82	50	50-40C	40	1.25	566	860257	499	758751
82	50	50-40C	40	1.50	677	857470	596	755208
82	50	50-40C	40	1.75	784	850984	697	756542
82	50	50-40C	40	2.00	889	844346	790	750488
82	50	50-40C	40	2.25	996	840709	888	749628
82	50	50-40C	40	2.50	1113	845424	981	745257
83	50	50-30C	30	0.25	139	1057372	112	853512
83	50	50-30C	30	0.50	249	947200	225	855852
83	50	50-30C	30	0.75	372	941394	330	834881
83	50	50-30C	30	1.00	492	934449	436	828010
83	50	50-30C	30	1.25	614	932987	546	829130
83	50	50-30C	30	1.50	734	929433	652	825433
83	50	50-30C	30	1.75	843	914610	751	815197
83	50	50-30C	30	2.00	957	909309	851	808452
83	50	50-30C	30	2.25	1093	922839	976	824283
83	50	50-30C	30	2.50	1217	924456	1078	819439
84	50	50-20C	20	0.25	116	885129	105	795998
84	50	50-20C	20	0.50	225	853169	200	761451
84	50	50-20C	20	0.75	332	840030	294	745867
84	50	50-20C	20	1.00	441	837634	389	739095
84	50	50-20C	20	1.25	549	834287	484	736089

84	50	50-20C	20	1.50	652	825438	575	727864
84	50	50-20C	20	1.75	756	820152	706	765992
84	50	50-20C	20	2.00	857	814414	805	764205
84	50	50-20C	20	2.25	987	833322	904	763002
84	50	50-20C	20	2.50	1107	841231	997	757882

B.3 RAW FLOWRATE DATA FOR VAA-COATED PCTE

RAW PERMEABILITY DATA ON VAA-COATED PCTE					
Exp. #	**Pore size,nm**	**Coating thickness,nm**	**P (psi)**	**Flow rate**	**Permeability (Barrer)**
23	50	40	0.25	126	959324
23	50	40	0.5	235	892733
23	50	40	0.75	341	864108
23	50	40	1	451	856636
23	50	40	1.25	555	843544
23	50	40	1.5	661	837071
23	50	40	1.75	766	831852
23	50	40	2	877	832975
23	50	40	2.25	979	826417
23	50	40	2.5	1073	815049
23	50	40	2.75	1187	819824
23	50	40	3	1296	820627
23	50	40	3.25	1388	811502
23	50	40	3.5	1517	823280
23	50	40	3.75	1642	831866
23	50	40	4	1742	827434
25	50	20	0.25	131	997054
25	50	20	0.5	255	969328
25	50	20	0.75	379	959941
25	50	20	1	493	936439
25	50	20	1.25	613	931048
25	50	20	1.5	734	929190
25	50	20	1.75	853	925985
25	50	20	2	995	945153
25	50	20	2.25	1111	937791
25	50	20	2.5	1220	927074
25	50	20	2.75	1361	940497
25	50	20	3	1532	970269
25	50	20	3.25	1621	947415
25	50	20	3.5	1739	944066
25	50	20	3.75	1898	961299
25	50	20	4	2037	967291
29	50	10	0.25	157	1196799
29	50	10	0.5	303	1150301
29	50	10	0.75	449	1138415
29	50	10	1	593	1127436
29	50	10	1.25	748	1136142
29	50	10	1.5	889	1126114
29	50	10	1.75	1031	1118750

29	50	10	2	1174	1115324
29	50	10	2.25	1335	1127271
29	50	10	2.5	1386	1053025
29	50	10	2.75	1509	1042531
30	50	20	0.25	135	1028497
30	50	20	0.5	268	1016618
30	50	20	0.75	389	985980
30	50	20	1	519	986704
30	50	20	1.25	645	980503
30	50	20	1.5	782	990272
30	50	20	1.75	949	1030333
30	50	20	2	1018	966628
30	50	20	2.25	1132	955498
30	50	20	2.5	1264	960380
30	50	20	2.75	1381	953752
30	50	20	3	1497	947993
30	50	20	3.25	1571	918131
31	50	30	0.25	99	749158
31	50	30	0.5	186	707272
31	50	30	0.75	274	695118
31	50	30	1	362	688141
31	50	30	1.25	452	687166
31	50	30	1.5	539	682862
31	50	30	1.75	625	678191
31	50	30	2	712	676393
31	50	30	2.25	796	672066
31	50	30	2.5	898	682343
31	50	30	2.75	999	690127
31	50	30	3	1129	714993
31	50	30	3.25	1176	687697
31	50	30	3.5	1293	701583
31	50	30	3.75	1374	696217
31	50	30	4	1534	728449
35	50	60	0.25	51	386124
35	50	60	0.5	100	379084
35	50	60	0.75	150	379200
35	50	60	1	195	370570
35	50	60	1.25	243	368640
35	50	60	1.5	290	367701
35	50	60	1.75	339	367611
35	50	60	2	387	367262
35	50	60	2.25	435	366937
35	50	60	2.5	481	365804
35	50	60	2.75	529	365250
35	50	60	3	580	367453

35	50	60	3.25	629	367861
35	50	60	3.5	676	367156
41	50	60	0.25	57	436552
41	50	60	0.5	110	417994
41	50	60	0.75	164	415030
41	50	60	1	216	411225
41	50	60	1.25	269	409497
41	50	60	1.5	323	409114
41	50	60	1.75	375	407542
41	50	60	2	429	407144
41	50	60	2.25	480	405469
41	50	60	2.5	533	405059
41	50	60	2.75	586	404772
41	50	60	3	639	404713
41	50	60	3.25	688	402384
41	50	60	3.5	749	406397
41	50	60	3.75	804	407229
48	50	60	0.25	36	276731
48	50	60	0.5	72	274793
48	50	60	0.75	108	272977
48	50	60	1	143	272037
48	50	60	1.25	178	269783
48	50	60	1.5	213	269559
48	50	60	1.75	247	268105
48	50	60	2	282	268196
48	50	60	2.25	316	267134
48	50	60	2.5	351	266410
36	50	50	0.25	85	646164
36	50	50	0.5	166	630464
36	50	50	0.75	248	627178
36	50	50	1	328	623541
36	50	50	1.25	409	621332
36	50	50	1.5	489	619308
36	50	50	1.75	570	619026
36	50	50	2	651	618547
36	50	50	2.25	728	614358
36	50	50	2.5	808	613817
36	50	50	2.75	890	614604
36	50	50	3	976	618005
36	50	50	3.25	1057	617910
36	50	50	3.5	1140	618907
42	50	50	0.25	91	692080
42	50	50	0.5	180	682978
42	50	50	0.75	269	681332
42	50	50	1	356	676861

42	50	50	1.25	441	670293
42	50	50	1.5	539	683128
42	50	50	1.75	631	684610
42	50	50	2	718	681750
42	50	50	2.25	818	690771
42	50	50	2.5	908	690184
42	50	50	2.75	978	675288
51	50	50	0.25	81	616118
51	50	50	0.5	159	604549
51	50	50	0.75	243	615330
51	50	50	1	311	591383
51	50	50	1.25	392	596177
51	50	50	1.5	471	596271
51	50	50	1.75	549	595939
51	50	50	2	627	595287
51	50	50	2.25	705	595179
51	50	50	2.5	779	591986
51	50	50	2.75	861	594669
51	50	50	3	935	592012
37	50	40	0.25	107	816809
37	50	40	0.5	211	800481
37	50	40	0.75	315	798370
37	50	40	1	418	794087
37	50	40	1.25	514	780577
37	50	40	1.5	617	781136
37	50	40	1.75	717	778384
37	50	40	2	842	799327
37	50	40	2.25	945	798046
37	50	40	2.5	1053	800448
37	50	40	2.75	1174	810813
37	50	40	3	1243	787291
43	50	40	0.25	118	897176
43	50	40	0.5	228	866002
43	50	40	0.75	338	856019
43	50	40	1	448	851513
43	50	40	1.25	558	847308
43	50	40	1.5	665	842079
43	50	40	1.75	773	838708
43	50	40	2	883	838872
43	50	40	2.25	1016	857785
52	50	40	0.25	109	829617
52	50	40	0.5	221	838825
52	50	40	0.75	325	823911
52	50	40	1	433	823104
52	50	40	1.25	538	817675

52	50	40	1.5	646	818188
52	50	40	1.75	747	810520
52	50	40	2	857	814195
52	50	40	2.25	965	814727
52	50	40	2.5	1071	813950
52	50	40	2.75	1167	806516
52	50	40	3	1286	814638
38	50	30	0.25	119	904666
38	50	30	0.5	243	923466
38	50	30	0.75	374	947139
38	50	30	1	505	960267
38	50	30	1.25	611	928021
38	50	30	1.5	738	934698
38	50	30	1.75	846	917896
38	50	30	2	962	914225
38	50	30	2.25	1084	915420
38	50	30	2.5	1206	916282
38	50	30	2.75	1325	915408
44	50	30	0.5	233	884074
44	50	30	0.75	344	871237
44	50	30	1	458	870903
44	50	30	1.25	569	864009
44	50	30	1.5	678	859224
44	50	30	1.75	794	862020
44	50	30	2	898	852924
44	50	30	2.25	1004	847722
44	50	30	2.5	1126	855770
44	50	30	2.75	1234	852535
39	50	20	0.25	135	1025046
39	50	20	0.5	264	1002055
39	50	20	0.75	391	989851
39	50	20	1	526	999507
39	50	20	1.25	652	990730
39	50	20	1.5	780	987894
39	50	20	1.75	902	979180
39	50	20	2	1033	980937
39	50	20	2.25	1170	987528
39	50	20	2.5	1286	977190
45	50	20	0.25	133	1009175
45	50	20	0.5	263	998540
45	50	20	0.75	387	981389
45	50	20	1	515	979260
45	50	20	1.25	643	976726
45	50	20	1.5	764	967787
45	50	20	1.75	891	966967

45	50	20	2	1014	963027
45	50	20	2.25	1138	960588
45	50	20	2.5	1268	963567
40	50	10	0.25	138	1050572
40	50	10	0.5	271	1028637
40	50	10	0.75	404	1022322
40	50	10	1	533	1013010
40	50	10	1.25	663	1007589
40	50	10	1.5	794	1005147
40	50	10	1.75	920	998983
40	50	10	2	1048	995687
40	50	10	2.25	1180	996125
46	50	10	0.25	116	881590
46	50	10	0.5	233	884152
46	50	10	0.75	350	886793
46	50	10	1	466	884694
46	50	10	1.25	578	878317
46	50	10	1.5	696	881149
46	50	10	1.75	808	877113
46	50	10	2	921	874390
46	50	10	2.25	1051	887528
46	50	10	2.5	1171	890162

APPENDIX C

PERMEABILITY DATA

PERMEABILITY DATA FROM LINEAR REGRESSION OF F VS. P CURVES								
Sample	Pore size	Coating	Coating Thickness	slope O2	O2 Perm	slope CO2	CO2 Perm	pO2/PCO2
60A	50	C6F14	60	301	572442	275	522708	1.10
50A	50	C6F14	50	345	654928	315	598564	1.09
40A	50	C6F14	40	378	718341	330	626489	1.15
30A	50	C6F14	30	443	841386	397	754208	1.12
20A	50	C6F14	20	466	885478	410	779018	1.14
60A	50	VAA	60	193	367254			
50A	50	VAA	50	325	617504			
40A	50	VAA	40	419	795393			
30A	50	VAA	30	484	919692			
20A	50	VAA	20	518	983732			
10A	50	VAA	10	527	1001095			
60B	50	VAA	60	214	405894			
50B	50	VAA	50	359	682417			
40B	50	VAA	40	446	847199			
30B	50	VAA	30	450	855634			
20B	50	VAA	20	509	966083			
10B	50	VAA	10	465	883331			
60C	50	VAA	60	141	268088	112	213281	
50C	50	VAA	50	313	594327	293	557435	1.07
40C	50	VAA	40	428	813498	370	702041	1.16
30C	50	VAA	30	456	865360	398	755518	1.15
20C	50	VAA	20	514	976608	443	841519	1.16
40nm	50	VAA	40	434	825276			
30nm	50	VAA	30	525	998245			
20nm	50	VAA	20	500	950278			
10nm	50	VAA	10	574	1090876			
20nm	50	VAA	20	503	955768			
blank	100		0	1264	2400485			
U6	50		0	606	1151268			
U7	50		0	569	1080826			
U8	50		0	569	1080408			
U9	50		0	561	1065306			
U10	50		0	567	1076476			
100A	100	C6F14	100	742	1410238	731	1388752	1.02
80A	100	C6F14	80	963	1829677	843	1600684	1.14
60A	100	C6F14	60	1112	2112108	979	1859198	1.14
40A	100	C6F14	40	1154	2192846	1053	2000404	1.10
20A	100	C6F14	20	1292	2453677	1158	2200065	1.12
10C	50	C6F`14	10	467	887454	410	778372	1.14
20B	50	C6F14	20	439	834718	399	757874	1.10
30B	50	C6F14	30	498	946554	433	823015	1.15
40B	50	C6F14	40	472	896819	416	791138	1.13
50B	50	C6F14	50	433	822350	380	721494	1.14

60B	50	C6F14	60	264	500728	240	455496	1.10
20B	100	C6F14	20	1264	2401435	1085	2061195	1.17
40B	100	C6F14	40	1158	2200445	1015	1928975	1.14
60B	100	C6F14	60	968	1838586	885	1681726	1.09
80B	100	C6F14	80	951	1806424	859	1632657	1.11
100B	100	C6F14	100	918	1743144	831	1578268	1.10
60C	50	C6F14	60	382	726073	332	629757	1.15
50C	50	C6F14	50	445	844748	393	746381	1.13
40C	50	C6F14	40	447	848890	396	752441	1.13
30C	50	C6F14	30	486	922751	432	820470	1.12
20C	50	C6F14	20	437	830557	398	755898	1.10

APPENDIX D

CONTACT ANGLE DATA

RAW DATA OBTAINED FROM WATER CONTACT ANGLE EXPERIMENTS									
50nm Uncoated		**50nm Uncoated**		**100nm Uncoated**		**VAA 50-60B**		**VAA 50-10B**	
Contact angle (deg)	**Volume (uL)**	**Contact angle (deg)**	**Volume (uL)**	**Contact angle (deg)**	**Volume (uL)**	**Contact angle (deg)**	**Volume (uL)**	**Contact angle (deg)**	**Volume (uL)**
51	2	51	2	49	2	73	2	67	2
52	4	53	4	49	4	75	4	67	4
53	6	53	6	50	6	75	6	67	6
53	8	53	8	50	8	75	8	67	8
53	10	53	10	50	10	75	10	67	10
53	12	53	12	50	12	75	12	67	12
48	14	53	14	50	14	75	14	65	14
46	12	53	16	50	16	73	16	63	16
40	10	48	18	48	18	73	14	59	14
34	8	47	16	48	16	69	12	34	12
22	6	41	14	47	14	51	10	33	10
17	4	35	12	46	12	36	8	33	8
		26	10	45	10	25	6	33	6
		20	8	38	8	23	4	30	4
		13	6	31	6				2
		10	4	20	4				
C6F14 50-60A		**C6F14 100-20A**		**C6F14 50-20A**		**C6F14 100-100A**		**100nm blank**	
Contact angle (deg)	**Volume (uL)**	**Contact angle (deg)**	**Volume (uL)**	**Contact angle (deg)**	**Volume (uL)**	**Contact angle (deg)**	**Volume (uL)**	**Contact angle (deg)**	**time, s**
110	2	106	2	108	2	109	2	54	0
110	4	106	4	108	4	108	4	54	30
110	6	106	6	108	6	108	6	50	60
110	8	106	8	108	8	108	8	45	90
110	10	105	10	108	10	108	10	42	120
109	12	106	12	108	12	108	12	38	150
108	14	106	14	108	14	107	14	32	180
108	16	106	16	105	16	107	16	31	210
105	18	105	18	105	18	103	18	27	240
100	20	100	20	103	20	100	16	24	270
97	18	90	18	101	18	98	14	22	300

80	16	77	16	98	16	90	12	20	330
78	14	77	14	99	14	81	10		
72	12	77	12	80	12	80	8		
71	10	76	10	77	10	77	6		
			8	76	8	72	4		
			6	76	6	72	2		

RAW DATA OBTAINED FROM WATER CONTACT ANGLE EXPERIMENTS OF VAA COATINGS AT DIFFERENT CROSSLINK DENSITY

100-50A H					100-50A M				
Contact angle (deg)	Contact angle (deg)	Contact angle (deg)	Avg.	Volume (uL)	Contact angle (deg)	Contact angle (deg)	Avg.	Volume (uL)	
88	88	88	88.0	2	78	78	78	2	
88	88	88	88.0	4	78	78	78	4	
88	88	88	88.0	6	78	78	78	6	
88	88	88	88.0	8	78	78	78	8	
88	88	87	87.7	10	78	78	78	10	
87	88	88	87.7	12	77	78	77.5	12	
78	80	81	79.7	14	75	76	75.5	14	
75	77	81	77.7	16	70	73	71.5	16	
65	74	77	72.0	18	60	64	62	14	
50	67	74	63.7	16	46	52	49	12	
30	64	72	55.3	14	42	46	44	10	
	34	61	47.5	12	39	40	39.5	8	
	26	48	37.0	10		40	40	6	
		30	30.0	8		4	4	4	
		18	18.0	6		2	2		
				4					

				2					
100-50A L				**100-80A H**		**100-80A M**		**100-80A L**	
Contact angle (deg)	**Contact angle (deg)**	**Avg.**	**Volume (uL)**	**Contact angle (deg)**	**Volume (uL)**	**Contact angle (deg)**	**Volume (uL)**	**Contact angle (deg)**	**Volume (uL)**
72	74	73	2	73	2	76	2	76	2
72	74	73	4	73	4	76	4	76	4
72	74	73	6	73	6	76	6	76	6
72	74	73	8	73	8	77	8	76	8
72	74	73	10	73	10	77	10	76	10
72	73	72.5	12	71	12	75	12	76	12
71	73	72	14	69	14	75	14	70	14
60	69	64.5	16	70	12	63	12	60	12
56	60	58	14	63	10	60	10	57	10
50	60	55	10	47	8	43	8	48	8
40	50	45	8	34	6	43	6	37	6
30	36	33	6	30	4	40	4	20	4
29	28	28.5	4		2		2		2
	2	2							

REFERENCES

1. Pandey, P. and R.S. Chauhan, *Membranes for gas separation.* Progress in Polymer Science, 2001. **26**(6): p. 853-893.

2. Truskey, G.A., Yuan, Fan, and Katz, David F. , *Transport Phenomena in Biological Systems*. Pearson Prentics Hall Bioengineering. 2004: Pearson Education , Inc. 793.

3. Welty, J.R., Wicks, Charles E., Wilson, Robert E., and Rorrer, Gregory, *Fundamentals of Momentum, Heat, and Mass Transfer*. fourth ed. 2001, New York: John Wiley and Sons.

4. Seader, J.D.a.H., Ernest J., *Separation Process Principles*. 1998: John Wiley and Sons.

5. Mulder, M., *Basic Principles of membrane Technology*. 1st ed. 1996: Kluwer Academic Publishers.

6. Ley, V., *Gas Permeation Properties of Selected Pulsed Plasma Polymers*, in *Chemistry*. 2002, University of Texas at Arlington: Arlington.

7. Perry, R.H.a.G., Don W., *Perry's Chemical Engineers' Handbook.* Seventh ed. 1997.

8. de Gennes, P.-G., Brochard-Wyart, Francoise, and Quere, David, *Capillarity and Wetting Phenomena: Drops,Bubbles,Pearls, Waves*. 1st ed. 2004: Springer.

9. de Gennes, P.G., *Wetting: statics and dynamics.* Reviews of Modern Physics, 1985. **57**(3): p. 827.

10. Drummond, M., Domingo M. Braile, Domingo M., Lima-Oliveira,Ana Paula M. , Camim,Adalberto S., *Technological evolution of membrane oxygenators.* Brazilian Journal of Cardiovascular Surgery, 2005. **20**(4): p. 432-437.

11. Iwahashi, H., K. Yuri, and Y. Nosé, *Development of the oxygenator: past, present, and future.* Journal of Artificial Organs, 2004. **7**(3): p. 111-120.

12. Fournier, R.L., *Extracorporeal devices*, in *Basic transport phenomena in biomedical engineering*. 1999, Edwards Brothers: Lillington, NC.

13. Rao, V., et al., *Etched ion track polymer membranes for sustained drug delivery.* Radiation Measurements, 2003. **36**(1-6): p. 585-589.

14. Sterlitech. 2002 [cited 2007 March 13]; http://www.sterlitech.com/products/membranes/polycarbonate/PCTEFeatures.htm].

15. Acharya, N.K., et al., *Gas permeation study of Ti-coated, track-etched polymeric membranes.* Vacuum, 2006. **81**(3): p. 389-393.

16. Kulshrestha, V., et al., *Study of gas permeation for asymmetric track-etched polymer blends.* International Journal of Hydrogen Energy, 2006. **31**(10): p. 1266-1270.

17. Kulshrestha, V., et al., *Gas and ion transport through a track-etched large-area polymer film.* Desalination, 2006. **195**(1-3): p. 273-280.

18. Schofield, R.W., A.G. Fane, and C.J.D. Fell, *Gas and vapour transport through microporous membranes. I. Knudsen-Poiseuille transition.* Journal of Membrane Science, 1990. **53**(1-2): p. 159-171.

19. Tung, K.-L. and C.-J. Chuang, *Effect of pore morphology on fluid flow and particle deposition on a track-etched polycarbonate membrane.* Desalination, 2002. **146**(1-3): p. 129-134.

20. Vijay, Y.K., et al., *Characterization of track etched membranes by gas permeation.* International Journal of Hydrogen Energy, 2004. **29**(5): p. 515-519.

21. Han, L.M.a.T., Richard B, *Pulsed-plasma polymerization of 1-vinyl-2-pyrrolidone: Synthesis of a linear polymer.* Journal of Polymer Science: Part A: Polymer Chemistry, 1998. **36**(17): p. 3121-3129.

22. Rinsch, C.L., et al., *Pulsed Radio Frequency Plasma Polymerization of Allyl Alcohol: Controlled Deposition of Surface Hydroxyl Groups.* Langmuir, 1996. **12**(12): p. 2995-3002.

23. Kessler, L., et al., *Surface treatment of polycarbonate films aimed at biomedical application.* Journal of Biomaterials Science -- Polymer Edition, 2003. **14**(10): p. 1135.

24. Ley, V., Kruzic, Andrew P., and Timmons, Richard B., *Permeation rates of low molecular weight gases through a plasma synthesized allyl alcohol membrane.* Journal of Membrane Science, 2003. **226**(1-2): p. 213-226.

25. Thomes, B., *The Influence on Protein Adsorption of Surface Chemistry and Surface Roughness Produced via the Pulsed Plasma Teqhnique*, in *Biomedical Engineering*. 1998, Uniiversity of Texas at Arlington: Arlington. p. 70.

26. Zhang, J., et al., *The characterization of structure-tailored plasma films deposited from the pulsed RF discharge.* Thin Solid Films, 2003. **435**(1-2): p. 108-115.

27. Yasuda, H., *Plasma Polymerization*. 1985, Orlando, FL: Academic Press.

28. Bhattacharyya, D., et al., *A New Class of Thin Film Hydrogels Produced by Plasma Polymerization.* 2007. **19**(9): p. 2222-2228.

29. Chen, T.N., et al., *Effects of plasma pretreatment on silicon nitride barrier films on polycarbonate substrates.* Thin Solid Films, 2006. **514**(1-2): p. 188-192.

30. Chen, X., et al., *Pulsed Plasma Polymerization of Tetramethyltin: Nanoscale Compositional Control of Film Chemistry.* Chemistry of Materials 1996. **8**(5): p. 1067-1077.

31. Poncin-Epaillard, F. and G. Legeay, *Surface engineering of biomaterials with plasma techniques.* Journal of Biomaterials Science -- Polymer Edition, 2003. **14**(10): p. 1005.

32. Teare, D.O.H., et al., *Pulsed Plasma Deposition of Super-Hydrophobic Nanospheres.* Chemistry of Materials, 2002. **14**(11): p. 4566-4571.

33. Sakata, J., Yamamoto, Minoru, and Hirai, Masana *Plasma polymerized membranes and gas permeability. II.* Journal of Applied Polymer Science, 1986. **31**(7): p. 1999-2006.

34. Sakata, J., ,Hirai , Masana,and Yamamoto,Minoru *Plasma-polymerized membranes and gas permeability III.* Journal of Applied Polymer Science, 1987. **34**(8): p. 2701-2711.

35. Sakata, J., Yamamoto, Minoru, and Tajima, Ichiro *Plasma polymerization of mixed monomer gases.* Journal of Polymer Science: Part A: Polymer Chemistry, 1988. **26**(7): p. 1721-1731.

36. Sakata, J., Yamamoto,Minoru,and Hirai, Masana *Plasma-polymerized membranes and gas permeability. IV.* Journal of Applied Polymer Science, 1989. **37**(9): p. 2773-2779.

37. Lue, S.J., et al., *Thermally on-off switching membranes of poly(N-isopropylacrylamide) immobilized in track-etched polycarbonate films.* Journal of Membrane Science. In Press, Corrected Proof.

38. Xie, R., et al., *Characterization of microstructure of poly(N-isopropylacrylamide)-grafted polycarbonate track-etched membranes prepared by plasma-graft pore-filling polymerization.* Journal of Membrane Science, 2005. **258**(1-2): p. 157-166.

39. Yamamoto, M., Sakata , Jiro and Hirai,Masana, *Plasma polymerized membranes and gas permeability. I.* Journal of Applied Polymer Science, 1984. **29**(10): p. 2981-2987.

40. Bird, B.R., Stewart, Warren E.,and Lightfoot, Edwin N., *Transport Phenomena*. second ed. 2002, New York: John wiley and Sons.

41. Altena, F.W., et al., *Some comments on the applicability of gas permeation methods to characterize porous membranes based on improved experimental accuracy and data handling.* Journal of Membrane Science, 1983. **12**(3): p. 313-322.

42. Hynes, A.M., M.J. Shenton, and J.P.S. Badyal, *Pulsed Plasma Polymerization of Perfluorocyclohexane.* Macromolecules, 1996. **29**(12): p. 4220-4225.

43. Oh, S.-J. and W.P. Zurawsky, *Gas permeation through poly(dimethylsiloxane)-plasma polymer composite membranes.* Journal of Membrane Science, 1996. **120**(1): p. 89-99.

BIOGRAPHICAL INFORMATION

Christopher Chapman was born and raised in South Texas. After receiving his GED, he attended community college for two years. He received his Bachelor's of Science Degree in Chemical Engineering from Texas A&M Kingsville in May 2004. He hopes to complement it with a Master's of Science Degree in Biomedical Engineering and gain industrial research and development experience specializing in medical devices, particularly mass transfer applications.